MDPI

Article

Single VDGA-Based Mixed-Mode Universal Filter and Dual-Mode Quadrature Oscillator

Natchanai Roongmuanpha [ID], Worapong Tangsrirat *[ID] and Tattaya Pukkalanun

School of Engineering, King Mongkut's Institute of Technology Ladkrabang (KMITL), Bangkok 10520, Thailand; natchanai.roo@gmail.com (N.R.); tattaya.pu@kmitl.ac.th (T.P.)
* Correspondence: worapong.ta@kmitl.ac.th

Abstract: This article presents the circuit designs for a mixed-mode universal biquadratic filter and a dual-mode quadrature oscillator, both of which use a single voltage differencing gain amplifier (VDGA), one resistor, and two capacitors. The proposed circuit has the following performance characteristics: (i) simultaneous implementation of standard biquadratic filter functions with three inputs and two outputs in all four possible modes, namely, voltage-mode (VM), current-mode (CM), trans-admittance-mode (TAM), and trans-impedance-mode (TIM); (ii) electronic adjustment of the natural angular frequency and independently single-resistance controllable high-quality factor; (iii) performing a dual-mode quadrature oscillator with simultaneous voltage and current output responses; (iv) orthogonal resistive and/or electronic control of the oscillation condition and frequency; (v) employing all grounded passive components in the quadrature oscillator function; and (vi) simpler topology due to the use of a single VDGA. VDGA non-idealities and parasitic elements are also investigated and analyzed in terms of their influence on circuit performance. To prove the study hypotheses, computer simulations with TSMC 0.18 μm CMOS technology and experimental confirmatory testing with off-the-shelf integrated circuits LM13600 have been performed.

Keywords: voltage differencing gain amplifier (VDGA); mixed-mode; dual-mode; universal biquadratic filter; voltage-mode (VM); current-mode (CM); trans-admittance-mode (TAM); trans-impedance-mode (TIM); quadrature oscillator

1. Introduction

Universal filters are useful active filters that permit all the five typical biquadratic filter functions simultaneously, namely low-pass (LP), band-pass (BP), high-pass (HP), band-stop (BS), and all-pass (AP) responses with the same topology. These circuits are frequently used in the design of a wide variety of electronic instruments, data communications, and control systems since they enable the implementation of various filtering functions based on port selections. In many analog signal processing applications, an active mixed-mode universal biquadratic filter (MUBF) with input voltages and/or currents, and output voltages and/or currents, is necessarily required. Over the last decade, numerous universal biquad filter realizations in mixed-mode operations based on different active components have already been developed in [1–31].

Two periodic waveforms having a 90° phase difference, known as a quadrature oscillator (QO), are frequently required in the design of electronic communication systems. QOs have applications in communication systems to operate quadrature mixers, in instrumentation and measurement systems to test and diagnose electronic devices and circuits, as well as in single-sideband generators. Interesting QO circuits have been reported in the literature, which includes realizations using various active building blocks [32–40].

Note that the above-mentioned realizations only work with the mixed-mode universal biquad filter or the QO circuit. Interestingly, [41–50] suggest circuit realizations that can perform both universal biquad filter and QO with the same circuit design. A comparison of available

related works is made in Table 1. A thorough examination of Table 1 shows that the MUBF realizations in [2,6,8,11,16,19,20,24,41–50] were unable to realize the various filter functions in all four possible operation modes, including voltage-mode (VM), current-mode (CM), trans-admittance-mode (TAM), and trans-impedance-mode (TIM). Furthermore, the QOs in [44,47,49] only generated voltage-mode quadrature signals, while those in [42,43] generated current-mode quadrature signals. In certain modern electronic applications, a QO circuit that provides both voltage and current outputs simultaneously, called a dual-mode QO (DMQO), may be required. However, little effort has been made on the design of DMQO [32–40]. The realizations in [1,2,4–7,9–15,17–20,22,23,25,26,29–31,33,34,37,39,42–47,49,50] need two or more active components. Four or more passive components were used in the circuits described in [2–4,6,8,9,12–16,19,21–24,26,27,29,31,32,34,35,37,39,45,47,48]. Moreover, the inbuilt tunability feature is not provided for the approaches presented in [2–4,6,8,9,12,13,19,22,23,31,32,34,39,47]. The circuits in [2,6–8,10,13,18,21,23,28,31,40,42,43,48,50] also do not allow for independent tuning of the important characteristics, such as the natural angular frequency and quality factor for MUBF, or the oscillation condition and frequency for QO.

Table 1. Comparison of the proposed circuit to previous related MUBF and QO circuits in [1–50].

Ref./ Year	Working as Both MUBF and QO	No. of Active and Passive Used	MUBF				Independent Tunable Q	QO		Inbuilt Tunability	Technology	Supply Voltages (V)	Power Consumption (W)	Technology	Supply Voltages (V)
			Filter Function Realized					Type (VM/CM) and Number of Outputs	Independent Tuning of OC and OF						
			VM	CM	TAM	TIM									
[1]/2003	N	DO-CCCII = 4, C = 3	LP, BP, HP	LP, BP, HP	LP, BP, HP	LP, BP, HP	Y	–	–	Y	HF3 CMOS	±5	N/A	–	–
[2]/2006	N	UGC = 8, R = 7, C = 2	all five	all five	–	–	N	–	–	N	1.2 µm CMOS	±5, −2.35, −3.54	N/A	–	–
[3]/2009	N	FDCCII = 1, R = 3, C = 2	all five	all five	BP, HP	all five	Y	–	–	N	TSMC 0.25 µm	±1.25	N/A	–	–
[4]/2009	N	DVCC = 3, Rmos = 3, C = 2	LP, BP, BS	all five	all five	LP, BP	Y	–	–	N	TSMC 0.35 µm	±1.5, 0.75	5.76 m	–	–
[5]/2009	N	OTA = 5, C = 2	all five	all five	all five	all five	Y	–	–	Y	TSMC 0.35 µm	±1.65, −1	30.95 m	–	–
[6]/2009	N	MO-CCII = 3, R = 3, C = 2	–	all five	–	all five	N	–	–	N	TSMC 0.18 µm	±1.25, −0.65	N/A	–	–
[7]/2010	N	OTA = 3, DO-OTA = 1, MO-OTA = 1, C = 2	all five	all five	all five	all five	N	–	–	Y	TSMC 0.25 µm	±1.25	N/A	–	–
[8]/2010	N	SCFOA = 1, R = 3, C = 2	all five	LP, BP, BS	–	–	N	–	–	N	TSMC 0.25 µm	±1.25	2.53 m	–	–
[9]/2011	N	DDCC = 3, R = 4, C = 2	all five	all five	all five	all five	Y	–	–	N	TSMC 0.25 µm	±1.25, +0.41	N/A	–	–
[10]/2013	N	MO-CCCII = 4, C = 2	all five	all five	all five	all five	N	–	–	Y	AMS 0.35 µm	±1.25	N/A	–	–
[11]/2013	N	VDTA = 2, C = 2	all five	–	all five	–	Y	–	–	Y	TSMC 0.18 µm	±1.5	N/A	–	–
[12]/2016	N	FDCCII = 1, DDCC = 1, R = 6, C = 2	all five	all five	all five	all five	Y	–	–	N	TSMC 0.18 µm	±0.9, ±0.38	N/A	AD844	±15
[13]/2016	N	FDCCII = 2, R = 5, C = 2	all five	all five	all five	all five	N	–	–	N	TSMC 0.18 µm	±0.9	N/A	–	–
[14]/2016	N	DP-CCII = 6, MO-CCII = 2, R = 4, C = 2	all five	all five	all five	all five	Y	–	–	Y	TSMC 0.18 µm	±0.75	3.26 m	–	–
[15]/2016	N	DPCF = 5, VF = 2, switch = 3, R = 4, C = 2	all five	all five	all five	all five	Y	–	–	Y	TSMC 0.18 µm	±1.5	1.2 m	–	–
[16]/2016	N	VDTA = 1, R = 1, C = 3	LP, BP, HP	LP, BP, HP	–	–	Y	–	–	Y	TSMC 0.18 µm	±0.9	0.54 m	–	–

Table 1. *Cont.*

Ref./Year	Working as Both MUBF and QO	No. of Active and Passive Used	MUBF					QO		Inbuilt Tunability	Technology	Supply Voltages (V)	Power Consumption (W)	Technology	Supply Voltages (V)
			Filter Function Realized				Independent Tunable Q	Type (VM/CM) and Number of Outputs	Independent Tuning of OC and OF						
			VM	CM	TAM	TIM									
[17]/2017	N	CCCCTA = 3, C = 2	all five	all five	all five	LP, BP, HP	Y	–	–	Y	TSMC 0.18 μm	±0.9	1.99 m	–	–
[18]/2017	N	MI-OTA = 3, MO-OTA = 3, C = 2	all five	all five	all five	all five	N	–	–	Y	TSMC 0.18 μm	±0.5	75 μ	–	–
[19]/2017	N	DVCC = 1, MO-CCII = 1, R = 4, C = 2	–	all five	–	all five	Y	–	–	N	TSMC 0.18 μm	±0.9, ±0.38	N/A	–	–
[20]/2017	N	OTA = 1, DO-OTA = 3, switch = 1, C = 2	–	LP, BP, HP	LP, BP, HP	–	Y	–	–	Y	TSMC 0.35 μm	N/A	1.3 m	–	–
[21]/2017	N	DXCCDITA = 1, R = 2, C = 2	all five	all five	BP, HP	all five	N	–	–	Y	TSMC 0.35 μm	±1.5, +0.55	N/A	AD844, LM13700	±5
[22]/2018	N	FDCCII = 2, R = 4, C = 2	all five	all five	all five	all five	Y	–	–	N	TSMC 0.18 μm	±0.9	1.32 m	–	–
[23]/2019	N	VCII = 3, I-CB = 1, R = 3, C = 3	all five	all five	all five	all five	N	–	–	N	TSMC 0.18 μm	±0.9	1.47 μ	–	–
[24]/2019	N	VD-DXCC = 1, R = 2, C = 2	all five	all five	–	–	Y	–	–	Y	PDK 0.18 μm	±1.25	2.237 m	–	–
[25]/2020	N	OTA = 5, C = 2	all five	all five	all five	all five	Y	–	–	Y	ADE 0.18 μm	±0.9, −0.36	0.191 m	–	–
[26]/2020	N	EXCCTA = 2, switch = 1, R = 4, C = 2	all five	all five	all five	all five	Y	–	–	Y	PDK 0.18 μm	±1.25	N/A	–	–
[27]/2021	N	VD-EXCCII = 1, R = 3, C = 3	all five	all five	all five	all five	Y	–	–	Y	PDK 0.18 μm	±1.25	5.76 m	–	–
[28]/2021	N	EX-CCCII = 1, R = 1, C = 2	all five	all five	all five	BP, HP	N	–	–	Y	TSMC 0.18 μm	±0.5	1.35 m	AD844	±8
[29]/2021	N	VDBA = 2, R = 2, C = 2	all five	all five	all five	LP, BP	Y	–	–	Y	TSMC 0.18 μm	±0.75	0.373 m	LT1228	±5
[30]/2022	N	VDBA = 3, R = 1, C = 2	all five	all five	all five	all five	Y	–	–	Y	PDK 0.18 μm	±1.25	5.482 m	CA3080, LF356	±5
[31]/2022	N	DVCC = 3, R = 4, C = 2	LP, BP, HP	all five	BP, HP	LP, BP, HP	N	–	–	N	TSMC 0.18 μm	±1.25, +0.55	8.47 m	AD844	±12
[32]/2006	N	FDCCII = 1, R = 3, C = 2	–	–	–	–	– –	VM/CM, VM = 2, CM = 2	Y	N	TSMC 0.18 μm	±2.5	118.1 m	–	–

Table 1. *Cont.*

Ref./Year	Working as Both MUBF and QO	No. of Active and Passive Used	MUBF					QO		Inbuilt Tunability	Technology	Supply Voltages (V)	Power Consumption (W)	Technology	Supply Voltages (V)
			Filter Function Realized				Independent Tunable Q	Type (VM/CM) and Number of Outputs	Independent Tuning of OC and OF						
			VM	CM	TAM	TIM									
[33]/2009	N	CDTA = 2, R = 1, C = 2	–	–	–	–	– –	VM/CM, VM = 2, CM = 2	Y	Y	MIETEC 0.5 µm	N/A	N/A	–	–
[34]/2009	N	DVCC = 3, R = 3, C = 3	–	–	–	–	– –	VM/CM, VM = 5, CM = 2	Y	N	MIETEC 0.5 µm	N/A	N/A	–	–
[35]/2014	N	DVCCTA = 1, R = 2, C = 2	–	–	–	–	– –	VM/CM, VM = 2, CM = 2	Y	Y	TSMC 0.18 µm	±0.9, −0.5	2.283 m	–	–
[36]/2016	N	CCCTA = 1, C = 2	–	–	–	–	– –	VM/CM, VM = 2, CM = 2	Y	Y	BJT, TSMC 0.35 µm	±1	N/A	–	–
[37]/2016	N	VDCC = 2, R = 2, C = 2	–	–	–	–	– –	VM/CM, VM = 2, CM = 3	Y	Y	TSMC 0.18 µm	±0.9	N/A	–	–
[38]/2017	N	VDTA = 1, C = 2	–	–	–	–	– –	VM/CM, VM = 2, CM = 2	Y	Y	TSMC 0.25 µm	±1.5	2.09 m	–	–
[39]/2020	N	DX-MOCCII = 2, Rmos = 1, R = 2, C = 2	–	–	–	–	– –	VM/CM, VM = 4, CM = 3	Y	N	TSMC 0.25 µm	±1.25, −0.3, +0.81	6.87 m	AD844	±9.5
[40]/2022	N	VDGA = 1, R = 1, C = 2	–	–	–	–	– –	VM/CM, VM = 2, CM = 2	N	Y	TSMC 0.35 µm	±1.5	1.36 m	–	–
[41]/2011	Y	DVCCCTA = 1, C = 2	LP, BP	–	–	–	Y	VM/CM, VM = 2, CM = 2	Y	Y	TSMC 0.25 µm	±1.25	N/A	–	–
[42]/2014	Y	CDTA = 2, C = 2	–	all five	–	–	N	CM, CM = 2	N	Y	TSMC 0.18 µm	±1.5	N/A	AD844, CA3080	±12
[43]/2014	Y	CDTA = 3, C = 2	–	all five	–	–	N	CM, CM = 4	Y	Y	MIETEC 0.5 µm	±2.5	19.6 m	–	–
[44]/2017	Y	VDDDA = 3, R = 1, C = 2	all five	–	–	–	Y	VM, VM = 2	Y	Y	TSMC 0.18 µm	±0.9	0.343 m	AD830, LM13700	±5
[45]/2017	Y	VDCC = 2, switch = 3, R = 2, C = 2	–	all five	–	–	Y	VM/CM, VM = 2, CM = 2	Y	Y	TSMC 0.18 µm	±0.9	N/A	OPA860	N/A
[46]/2019	Y	CCFTA = 2, C = 2	–	all five	–	–	Y	VM/CM VM = 2 CM = 4	Y	Y	TSMC 0.18 µm	±1	2 m	–	–
[47]/2020	Y	CCII = 2, R = 3, C = 2	all five	–	–	–	Y	VM, VM = 2	Y	N	IBM 0.13 µm	±0.75, +0.23	5.03 m	AD844	±6

Table 1. *Cont.*

Ref./ Year	Working as Both MUBF and QO	No. of Active and Passive Used	MUBF				Independent Tunable Q	QO			Technology	Supply Voltages (V)	Power Consumption (W)	Technology	Supply Voltages (V)
			Filter Function Realized					Type (VM/CM) and Number of Outputs	Independent Tuning of OC and OF	Inbuilt Tunability					
			VM	CM	TAM	TIM									
[48]/2020	Y	VDGA = 1, R = 2, C = 2	LP, BP, HP	LP, BP, HP	–	–	Y	VM/CM, VM = 2, CM = 2	N	Y	TSMC 0.25 µm	±1	1.49 m	–	–
[49]/2021	Y	MI-OTA = 3, OTA = 1, C = 2	all five	–	–	–	Y	VM, VM = 3	Y	Y	TSMC 0.18 µm	±1.2	96 µ	LM13700	±5
[50]/2021	Y	VDCC = 2, switch = 2, R = 1, C = 2	–	all five	–	–	N	VM/CM, VM = 2, CM = 2	Y	Y	TSMC 0.18 µm	±0.9	N/A	OPA860	N/A
This work	Y	VDGA = 1, R = 1, C = 2	all five	all five	all five	LP, BP	Y	VM/CM, VM = 2, CM = 3	Y	Y	TSMC 0.18 µm	±0.9	1.31 m	LM13600	±5

Notes: Y = Yes, N = No, N/A = not available, "–" = not realized, R = resistor, C = capacitor, Rmos = MOS-based electronic resistor, OTA = operational transconductance amplifier, DO-OTA = dual-output OTA, MO-OTA = multiple-output OTA, MI-OTA = multiple-input OTA, CCII = second-generation current conveyor, MO-CCII = multiple-output CCII, DP-CCII = digitally programmable current conveyor, DO-CCCII = dual-output second-generation current-controlled conveyor, MO-CCCII = multiple-outputs current-controlled conveyor, FDCCII = fully differential current conveyor, CFOA = current feedback operational amplifier, SCFOA = specific CFOA, UGC = unity-gain cell, DVCC = differential voltage current conveyor, DDCC = differential difference current conveyor, DVCCTA = differential voltage current conveyor transconductance amplifier, DVCCCTA = differential voltage current-controlled conveyor transconductance amplifier, CCCCTA = current controlled current conveyor transconductance amplifier, VDTA = voltage differencing transconductance amplifier, VDGA = voltage differencing gain amplifier, DPCF = digitally programmable current follower, VF = voltage follower, DXCCDITA = dual X current conveyor differential input transconductance amplifier, VCII = second-generation voltage conveyor, I-CB = inverting current buffer, VD-DXCC = voltage differencing dual X current conveyor, EXCCTA = extra X current conveyor transconductance amplifier, VD-EXCCII = voltage differencing extra X CCII, EX-CCCII = extra X CCCII, VDBA = voltage differencing buffered amplifier, CDTA = current differencing transconductance amplifier, CCFTA = current-controlled current follower transconductance amplifier, VDDDA = voltage differencing differential difference amplifier.

A voltage differencing gain amplifier (VDGA), a recently introduced active element, was introduced in 2013 [51], and has since been used in a variety of analog signal processing applications [52–56]. As previously stated, we found that no attempts have been made to use a single VDGA to implement both MUBF and DMQO with the same configuration. Considering the growing interest in multiple-mode signal processing, this work therefore proposes a MUBF and DMQO circuit designed using a single VDGA. The circuit makes use of only one resistor and two capacitors as passive components. By significantly modifying the design, the proposed circuit can be categorized as either a MUBF or a DMQO. For the proposed mixed-mode filter, it can perform VM, CM, TAM, and TIM biquadratic filters with an orthogonally controlled the natural angular frequency and the quality factor. Furthermore, the high-Q filter may be easily implemented with a single resistor. For the proposed DMQO, the oscillation condition and the oscillation frequency are separately programmable. The performance of the proposed MUBF and DMQO circuit is illustrated by PSPICE simulation results. To further demonstrate the practicability of the circuit, the experimental test results using commercially available ICs are also conducted.

2. Overview of VDGA

The VDGA device, which was recently described in [51], is a versatile active element. A wide range of VDGA-based analog signal processing solutions, including active universal filters [52,53], quadrature oscillators [54,55], and tunable capacitance multiplier [56], have been developed in the technical literature. Its schematic representation is illustrated in Figure 1, with p and n representing high-impedance voltage input terminals, $z+$, $z-$, x, and o representing high-impedance current output terminals, and w representing a low-impedance voltage output terminal. The ideal terminal property of the VDGA element is represented by the matrix expression [51]:

$$\begin{bmatrix} i_{z+} \\ i_{z-} \\ i_x \\ v_w \\ i_o \end{bmatrix} = \begin{bmatrix} g_{mA} & -g_{mA} & 0 & 0 \\ -g_{mA} & g_{mA} & 0 & 0 \\ 0 & 0 & g_{mB} & 0 \\ 0 & 0 & \beta & 0 \\ 0 & 0 & 0 & -g_{mC} \end{bmatrix} \cdot \begin{bmatrix} v_p \\ v_n \\ v_{z+} \\ v_w \end{bmatrix}, \tag{1}$$

where g_{mk} (k = A, B, C) is the transconductance gain and β is the transfer voltage gain of the VDGA.
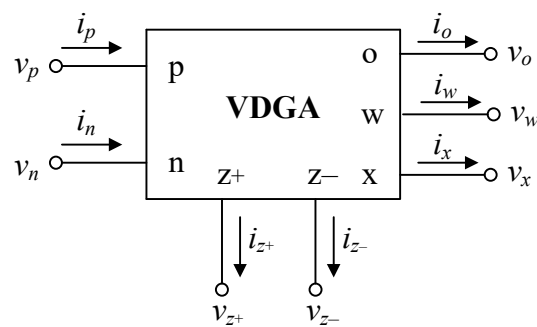

Figure 1. Schematic representation of the VDGA.

Figure 2 shows the probable CMOS-built VDGA internal circuit implementation, which comprises three voltage-controlled floating current sources M_{1k}–M_{9k}. Each M_{1k}–M_{9k} implements the corresponding independent adjustable transconductance g_{mk}, as written below [57]:

$$g_{mk} \cong \left(\frac{g_{1k}g_{2k}}{g_{1k} + g_{2k}} \right) + \left(\frac{g_{3k}g_{4k}}{g_{3k} + g_{4k}} \right), \tag{2}$$

where

$$g_{ik} = \sqrt{\mu C_{ox} \frac{W}{L} I_{Bk}}, \ (i = 1, \ 2, \ 3, \ 4), \tag{3}$$

μ is the effective channel electronic mobility, C_{ox} is the gate-oxide capacitance per unit area, and W and L are the respective channel width and length of M_{1k}–M_{4k}. Because each transconductance g_{ik} is proportional to the square root of the bias current I_{Bk}, the value of g_{mk} may be electronically scaled using Equations (2) and (3). A current-controlled voltage amplifier is also accomplished in Figure 2 by a pair of transconductors M_{1B}–M_{4B} and M_{1C}–M_{4C} with a voltage gain of $\beta = v_w/v_{z+} = g_{mB}/g_{mC}$.
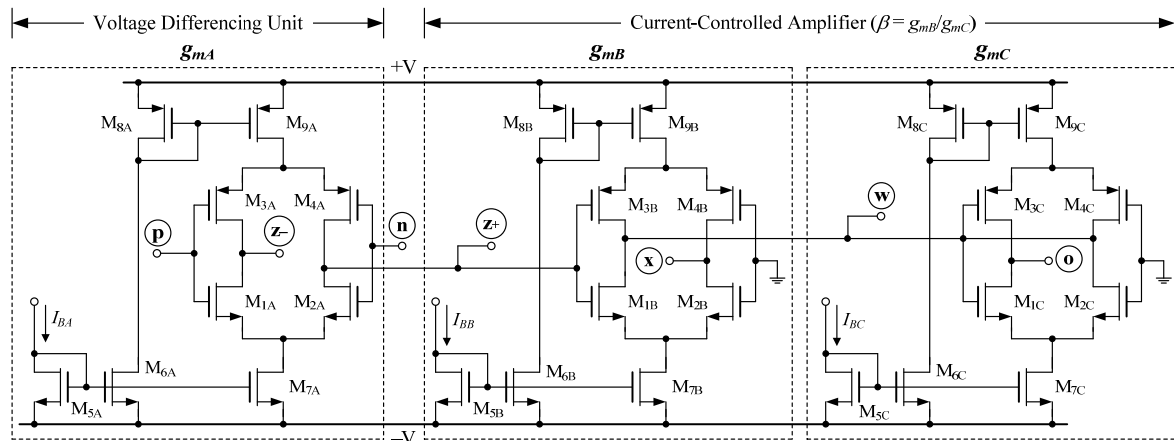
Figure 2. VDGA internal circuit implementation in CMOS technology.

3. Proposed Mixed-Mode Universal Biquadratic Filter

Figure 3 depicts the proposed universal filter configuration, which consists of a single VDGA, one resistor, and two capacitors. This configuration can be used to implement the mixed-mode universal biquad filter, which includes VM, CM, TAM, and TIM, by selecting appropriate input and output signals, as detailed below.
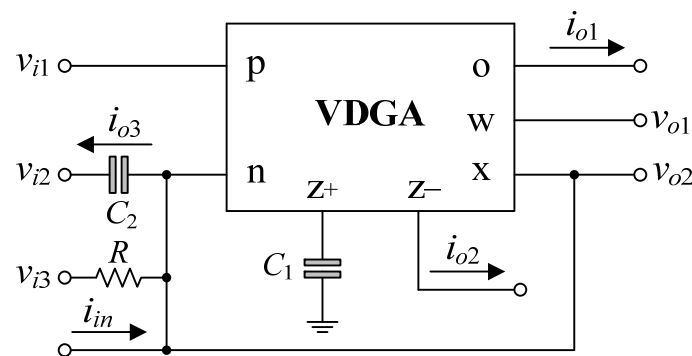
Figure 3. Proposed mixed-mode universal biquadratic filter.

➢ *VM universal biquadratic filter*: With $i_{in} = 0$, all the five general voltage-mode biquadratic filter functions for this three-input two-output universal filter can be achieved as follows.

● With $v_{in} = v_{i3}$ (input voltage) and $v_{i1} = v_{i2} = 0$ (grounded), the following LP and BP filter responses are obtained from v_{o1} and v_{o2}, respectively:

$$T_{VLP}(s) = \frac{v_{o1}}{v_{in}} = \left(-\frac{1}{g_{mC}R}\right)T_{LP}(s), \tag{4}$$

and

$$T_{VBP}(s) = \frac{v_{o2}}{v_{in}} = T_{BP}(s). \tag{5}$$

- With $v_{in} = v_{i2}$ and $v_{i1} = v_{i3} = 0$, the HP response is obtained from v_{o2}, as given by:

$$T_{VHP}(s) = \frac{v_{o2}}{v_{in}} = T_{HP}(s). \tag{6}$$

- With $v_{in} = v_{i1} = v_{i2}$, and $v_{i3} = 0$, the BS response is obtained from v_{o2}, as given by:

$$T_{VBS}(s) = \frac{v_{o2}}{v_{in}} = T_{BS}(s). \tag{7}$$

- With $v_{in} = v_{i1} = v_{i2} = -v_{i3}$, the AP response is also obtained from v_{o2}, as given by:

$$T_{VAP}(s) = \frac{v_{o2}}{v_{in}} = T_{AP}(s). \tag{8}$$

In Equations (4)–(8), the transfer functions $T_{LP}(s)$, $T_{BP}(s)$, $T_{HP}(s)$, $T_{BS}(s)$, and $T_{AP}(s)$, are as follows.

$$T_{LP}(s) = \frac{\left(\frac{g_{mA}g_{mB}}{C_1 C_2}\right)}{D(s)}, \tag{9}$$

$$T_{BP}(s) = \frac{\left(\frac{s}{RC_2}\right)}{D(s)}, \tag{10}$$

$$T_{HP}(s) = \frac{s^2}{D(s)}, \tag{11}$$

$$T_{BS}(s) = \frac{s^2 + \left(\frac{g_{mA}g_{mB}}{C_1 C_2}\right)}{D(s)}, \tag{12}$$

$$T_{AP}(s) = \frac{s^2 - \left(\frac{s}{RC_2}\right) + \left(\frac{g_{mA}g_{mB}}{C_1 C_2}\right)}{D(s)}, \tag{13}$$

and

$$D(s) = s^2 + \left(\frac{s}{RC_2}\right) + \left(\frac{g_{mA}g_{mB}}{C_1 C_2}\right). \tag{14}$$

Equation (4) reveals that the circuit implements the inverted LP filter function with a passband gain of $1/g_{mC}R$, whereas the others, represented by Equations (5)–(8), have a passband gain of unity. For the VM operation, no element-matching requirements are needed.

➢ *CM universal biquadratic filter*: The proposed circuit in Figure 3 can be changed into a CM universal biquad with $v_{i1} = v_{i2} = v_{i3} = 0$. The five generic current-mode biquad transfer functions realized by this configuration are expressed as follows.

$$T_{ILP}(s) = \frac{i_{o1}}{i_{in}} = T_{LP}(s), \tag{15}$$

$$T_{IBP}(s) = \frac{i_{o2}}{i_{in}} = (g_{mA}R)T_{BP}(s), \tag{16}$$

and

$$T_{IHP}(s) = \frac{i_{o3}}{i_{in}} = T_{HP}(s), \tag{17}$$

where the passband gain of the BP response is equal to $g_{mA}R$. Furthermore, the BS response may be realized by simply adding the currents i_{o1} and i_{o3} to realize the following current transfer function:

$$T_{IBS}(s) = \frac{i_{o1} + i_{o3}}{i_{in}} = T_{BS}(s). \tag{18}$$

Similarly, by retaining $g_{mA}R = 1$, the AP current response may be obtained by connecting the three currents i_{o1}, i_{o2}, and i_{o3} to obtain the following transfer function:

$$T_{IAP}(s) = \frac{i_{o1} - i_{o2} + i_{o3}}{i_{in}} = T_{AP}(s). \tag{19}$$

➤ *TAM universal biquadratic filter*: With $v_{in} = v_{i3}$, $v_{i1} = v_{i2} = 0$, and $i_{in} = 0$, the TAM filter functions are:

$$T_{YLP}(s) = \frac{i_{o1}}{v_{in}} = \left(\frac{1}{R}\right)T_{LP}(s), \tag{20}$$

$$T_{YBP}(s) = \frac{i_{o2}}{v_{in}} = g_{mA}T_{BP}(s), \tag{21}$$

$$T_{YHP}(s) = \frac{i_{o3}}{v_{in}} = \left(\frac{1}{R}\right)T_{HP}(s), \tag{22}$$

$$T_{YBS}(s) = \frac{(i_{o1} + i_{o3})}{v_{in}} = \left(\frac{1}{R}\right)T_{BS}(s), \tag{23}$$

and

$$T_{YAP}(s) = \frac{(i_{o1} - i_{o2} + i_{o3})}{v_{in}} = \left(\frac{1}{R}\right)T_{AP}(s). \tag{24}$$

Equation (21) represents the TAM filter function of the BP response with an electronically controlled passband gain of g_{mA}. The passband gains for the LP, HP, BS, and AP filter responses are equal to $1/R$. It should be noticed from Equation (24) that, in the case of AP filter realization, a simple element condition, $g_{mA}R = 1$, is necessary.

➤ *TIM universal biquadratic filter*: According to Figure 3, if $v_{i1} = v_{i2} = v_{i3} = 0$, the configuration is now operating in TIM universal filter. In this case, the two following TIM responses at voltage outputs v_{o1} and v_{o2} can simultaneously be obtained as:

$$T_{ZLP}(s) = \frac{v_{o1}}{i_{in}} = \left(-\frac{1}{g_{mC}}\right)T_{LP}(s), \tag{25}$$

and

$$T_{ZBP}(s) = \frac{v_{o2}}{i_{in}} = RT_{BP}(s). \tag{26}$$

Equations (25) and (26) express the TIM filter functions of the LP and BP filters with passband gains of $(-1/g_{mC})$ and R, respectively.

As a consequence, the proposed circuit shown in Figure 3 can be considered as a universal mixed-mode biquadratic filter. The natural angular frequency and the quality factor of this filter are given by [53].

$$\omega_o = 2\pi f_o = \sqrt{\frac{g_{mA}g_{mB}}{C_1 C_2}}, \tag{27}$$

and

$$Q = R\sqrt{\frac{g_{mA}g_{mB}C_2}{C_1}}. \tag{28}$$

It is important to note from Equation (27) that the ω_o can be electronically tuned by changing the transconductances g_{mA} and g_{mB}. In addition to Equation (28), the high-Q universal filter can be easily realized by tuning the resistor R without affecting the characteristic frequency ω_o.

4. Proposed Dual-Mode Quadrature Oscillator

In Figure 3, by taking $v_{i1} = v_{i2} = v_{i3} = i_{in} = 0$, and connecting terminal $z-$ to x of the VDGA, the proposed mixed-mode universal biquadratic filter can be worked as a

quadrature sinusoidal oscillator. Figure 4 shows the proposed dual-mode quadrature oscillator based on the proposed mixed-mode universal filter in Figure 3. It is worth noting that in this design, all of the passive components are grounded. The characteristic equation of the proposed dual-mode quadrature oscillator in Figure 4 is found as [54]:

$$s^2 + \left(\frac{1 - g_{mA}R}{RC_2} \right)s + \left(\frac{g_{mA}g_{mB}}{C_1 C_2} \right) = 0. \tag{29}$$
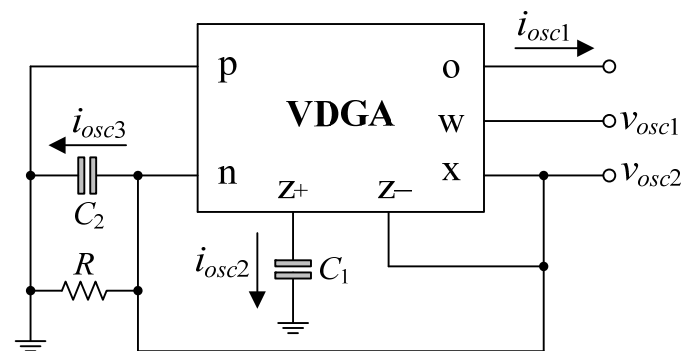
Figure 4. Proposed dual-mode quadrature oscillator.

From Equation (29), the oscillation condition (OC) and the oscillation frequency (OF) are evaluated by [55]:

$$\text{OC}: \ g_{mA}R = 1, \tag{30}$$

and

$$\text{OF}: \ \omega_{osc} = 2\pi f_{osc} = \sqrt{\frac{g_{mA}g_{mB}}{C_1 C_2}}. \tag{31}$$

As can be observed from Equations (30) and (31), the OC can be controlled simply by changing the value of a grounded resistor R without altering the OF, which can be tuned separately using the transconductance g_{mB}. As a result, the parameters OC and OF of the proposed quadrature oscillator in Figure 4 are orthogonal controllable.

For sinusoidal steady state, the relationship between the output voltages v_{osc1} and v_{osc2} is

$$v_{osc1} = \left(\frac{g_{mA}g_{mB}}{\omega_{osc}g_{mC}C_1} \right) e^{j90°} v_{osc2}. \tag{32}$$

Thus, the proposed circuit produces the two marked voltages v_{osc1} and v_{osc2} in quadrature signal.

Also from Figure 4, the output current relations from i_{osc1} to i_{osc2} and i_{osc3} at the OF are found as:

$$i_{osc1} = \left(\frac{g_{mB}}{\omega_{osc}C_1} \right) e^{j90°} i_{osc2} = \left(\frac{g_{mA}g_{mB}}{\omega_{osc}^2 C_1 C_2} \right) e^{j180°} i_{osc3}. \tag{33}$$

According to Equation (33), the phase differences between i_{osc1} and i_{osc2}, as well as i_{osc1} and i_{osc3}, are 90° and 180°, respectively. This demonstrates that the three output currents are not only 90° out of phase, but also 180° out of phase.

5. Non-Ideal Analyses

This section investigates the impact of VDGA non-idealities on the performance of the proposed mixed-mode universal biquad filter and dual-mode quadrature oscillator. In fact, the non-idealities of the VDGA arise mostly from two significant consequences. The first set of effects is caused by finite tracking errors, whereas the second group is caused by the existence of all VDGA terminal parasitics.

5.1. Effect of Finite Tracking Errors

Considering the tracking errors of the VDGA into account, the terminal property given by Equation (1) may be reformulated as [53–55]:

$$
\begin{bmatrix} i_{z+} \\ i_{z-} \\ i_x \\ v_w \\ i_o \end{bmatrix} = \begin{bmatrix} \alpha_A g_{mA} & -\alpha_A g_{mA} & 0 & 0 \\ -\alpha_A g_{mA} & \alpha_A g_{mA} & 0 & 0 \\ 0 & 0 & \alpha_B g_{mB} & 0 \\ 0 & 0 & \delta\beta & 0 \\ 0 & 0 & 0 & -\alpha_C g_{mC} \end{bmatrix} \cdot \begin{bmatrix} v_p \\ v_n \\ v_{z+} \\ v_w \end{bmatrix},
\tag{34}
$$

where α_k ($\alpha_k = 1 - \varepsilon_\alpha$) and δ ($\delta = 1 - \varepsilon_\delta$) denote the transconductance inaccuracy parameter and the parasitic voltage gain of the VDGA, respectively. These non-ideal parameters differ from unity due to the transfer errors ε_α ($|\varepsilon_\alpha| << 1$) and ε_δ ($|\varepsilon_\delta| << 1$).

In presence of the VDGA tracking defects, the expressions for the parameters ω_o and Q of the proposed mixed-mode universal biquad filter in Figure 3 are modified as:

$$
\omega_o = \sqrt{\frac{\alpha_A \alpha_B g_{mA} g_{mB}}{C_1 C_2}},
\tag{35}
$$

and

$$
Q = R\sqrt{\frac{\alpha_A \alpha_B g_{mA} g_{mB} C_2}{C_1}}.
\tag{36}
$$

Through the tracking error effects, the values of ω_o and Q clearly depart slightly from their ideal values. These variations may be accommodated by altering the transconductance gains g_{mA} and g_{mB} via the bias currents of VDGA.

For the proposed dual-mode quadrature oscillator in Figure 4, the modified OC and OF can be derived as:

$$
\text{OC}: \ \alpha_A g_{mA} R = 1,
\tag{37}
$$

and

$$
\text{OF}: \ \omega_{osc} = \sqrt{\frac{\alpha_A \alpha_B g_{mA} g_{mB}}{C_1 C_2}}.
\tag{38}
$$

It is evident that the non-ideal factors clearly cause the OC and OF parameters to deviate slightly. However, the OC and OF can still be altered through adjusting R and g_{mB}, respectively.

5.2. Effect of Parasitics

The non-ideal behavior model of the VDGA including finite parasitic impedances at each terminal is represented in Figure 5. These parasitics consist of resistance in parallel with capacitance for the p, n, $z+$, $z-$, x and o terminals, and serial resistance at the w terminal [53–55]. Because of the presence of these undesired parasitics, the circuit performance may differ from ideality. As a result, the suggested circuits in Figures 3 and 4, including the VDGA parasitics, must be thoroughly examined.

Using the non-ideal model of VDGA shown in Figure 5, the non-ideal ω_o and Q of the filter configuration in Figure 3 are found as:

$$
\omega_o = \sqrt{\frac{g_{mA} g_{mB} + \frac{1}{R' R_{z+}}}{C_1' C_2'}},
\tag{39}
$$

and

$$
Q = \left(\frac{R' R_{z+} C_1'}{R_{z+} C_1' + R' C_2'}\right)\sqrt{\frac{\left(g_{mA} g_{mB} + \frac{1}{R' R_{z+}}\right) C_2'}{C_1'}}.
\tag{40}
$$

where $R' = R \parallel R_n \parallel R_x$, $C_1' = C_1 + C_{z+}$, and $C_2' = C_2 + C_n + C_x$.
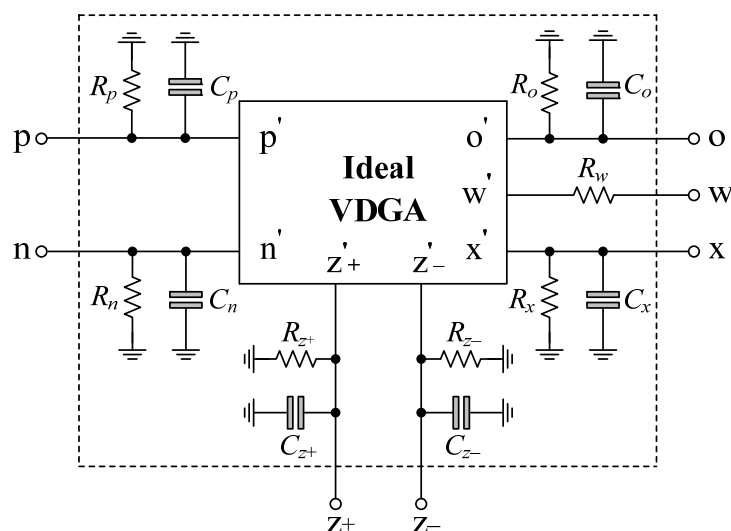
Figure 5. Non-ideal behavior model of the VDGA.

Similarly, the non-ideal OC and OF of the oscillator configuration in Figure 4 are also found as:

$$\text{OC}: \left(g_{mA} - \frac{C_2''}{R_{z+}C_1'} \right) R'' = 1, \tag{41}$$

and

$$\text{OF}: \ \omega_{osc} = \sqrt{\frac{g_{mA}g_{mB} + \left(\frac{1 - g_{mA}R''}{R''R_{z+}} \right)}{C_1'C_2''}}. \tag{42}$$

where $R'' = R \parallel R_n \parallel R_{z-} \parallel R_x$ and $C_2'' = C_2 + C_n + C_{x-} + C_x$. From Equations (39)–(42), the frequency characteristics of the proposed filter and oscillator circuits would be unaffected, if the following constraints were fulfilled:

$$\text{maximum } R \ll \text{ parasitic resistances } (R_n, R_{z\text{-}}, R_x), \tag{43}$$

and

$$\text{minimum } (C_1, C_2) \gg \text{ parasitic capacitances } (C_n, C_{z+}, C_{z\text{-}}, C_x). \tag{44}$$

6. Simulation Results

In this section, a PSPICE simulation program was carried out to demonstrate the performance of the proposed configurations in Figures 3 and 4. The VDGA was simulated using the CMOS circuit of Figure 2 with TSMC 0.18 μm transistor parameters, and with symmetrical supply voltages of ±0.9 V. Table 2 illustrates the aspect ratios of the CMOS transistors employed for the VDGA circuit in Figure 2. The capacitor settings for global simulations were $C_1 = C_2 = 50$ pF.

Table 2. Aspect ratios of the CMOS transistors of the VDGA in Figure 2.

Transistors	W (μm)	L (μm)
M_{1k}–M_{2k}	23.5	0.18
M_{3k}–M_{4k}	30	0.18
M_{5k}–M_{7k}	5	0.18
M_{8k}–M_{9k}	5.5	0.18

6.1. Simulation Verifications of the Proposed Mixed-Mode Universal Filter

The suggested mixed-mode universal filter in Figure 3 was performed with $g_{mA} = g_{mB} = g_{mC} = 1$ mA/V ($I_{BA} = I_{BB} = I_{BC} = 80$ μA), and $R = 1$ kΩ, to actualize all the four-mode

universal filter responses with f_o = 3.18 MHz and Q = 1. Figures 6–9 illustrate the simulated and theoretical frequency responses of VM, CM, TAM, and TIM filters, respectively. The disparity between simulated and theoretical gain responses in the HP filters of VM, CM, and TAM, as well as the BP filter of TIM, is greater in the low-frequency range of roughly 1 kHz to 100 kHz. This phenomenon may be explained by the fact that the input or output signals of the circuits were sensed with C_2 and R, introducing an undesirable pole that caused significant deviations in low operating frequencies. In Figures 6c and 7c, the phase shifting between input and output signals was measured as −190.70° and −192.74°, respectively, and the gain response was 0.84 dBV and 1.067 dBA down from zero for the frequency ranges varying from 1 kHz to 1 MHz. The simulated f_o and corresponding percentage errors are given in Table 3. It is to be observed that all simulation results are found to be in good consistent with the theoretical values. Figures 10–13 depict the transient responses of the proposed filter to the following input signals: (i) a 3.18 MHz sinusoidal input voltage signal with an amplitude of 100 mV (peak-to-peak) applied to the VM and TAM filters; and (ii) 3.18 MHz sinusoidal input current signal with an amplitude of 100 µA (peak-to-peak) applied to the CM and TIM filters. Table 4 shows the total harmonic distortions (THDs) and DC components of the VM, CM, TAM, and TIM outputs in Figures 10–13. As can be seen, the THD value is less than 1.92% in all four modes. Thus, there is no significant distortion in the biquad design. The entire power consumption of the circuit was 1.31 mW at ±0.9 V biased voltages.

(a)

(b)
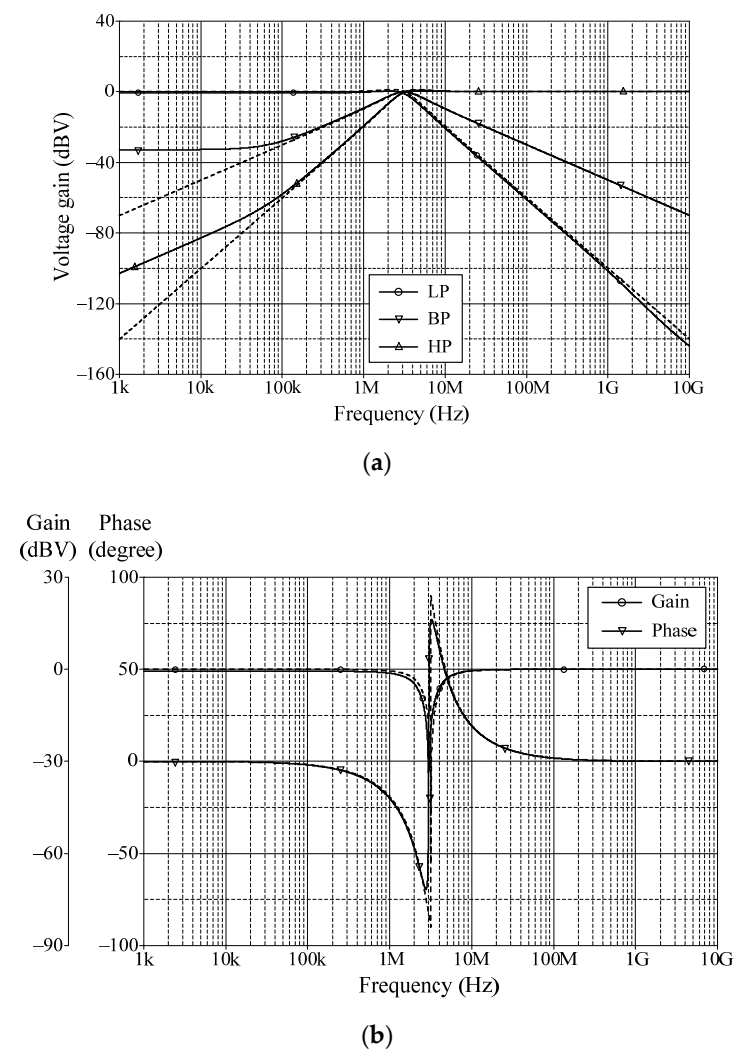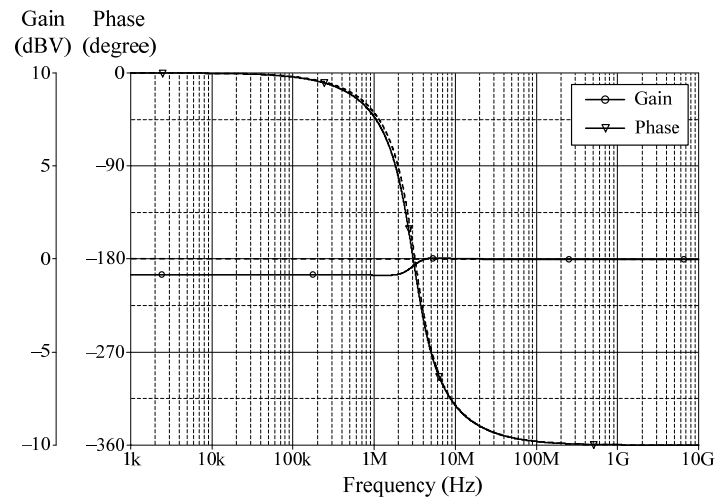
Figure 6. *Cont.*

(**c**)

Figure 6. Frequency characteristics for VM (simulated in solid line, theoretical in dashed line): (**a**) LP, BP, and HP; (**b**) BS; (**c**) AP.
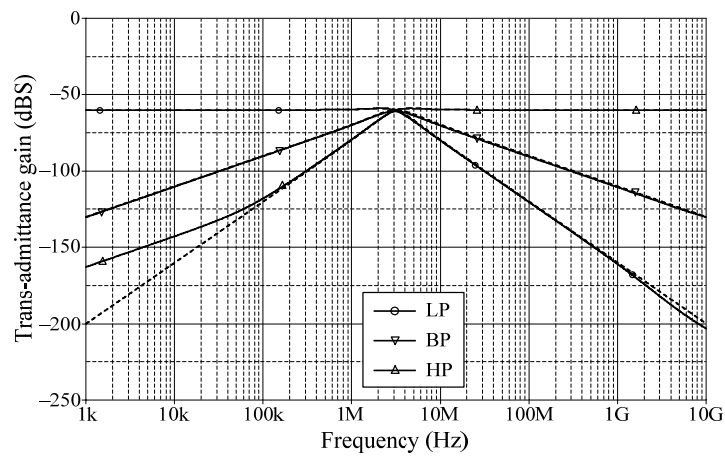

(**a**)

(**b**)

Figure 7. *Cont.*

(**c**)
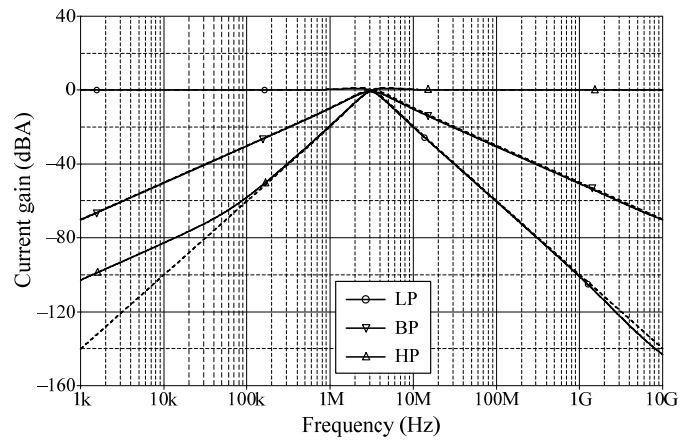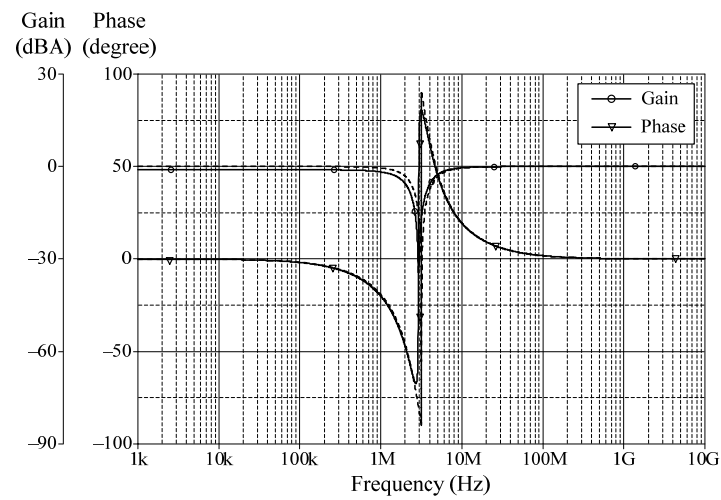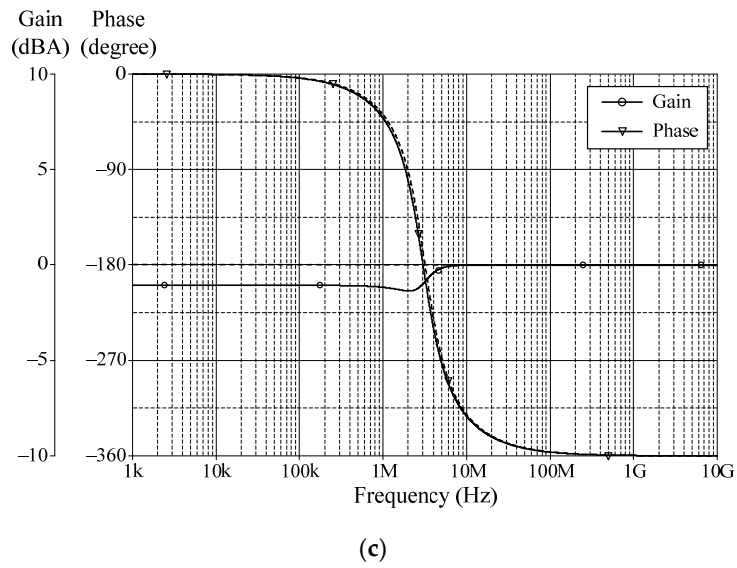
Figure 7. Frequency characteristics for CM (simulated in solid line, theoretical in dashed line): (**a**) LP, BP, and HP; (**b**) BS; (**c**) AP.

Figure 8. LP, BP, and HP frequency characteristics for TAM (simulated in solid line, theoretical in dashed line).
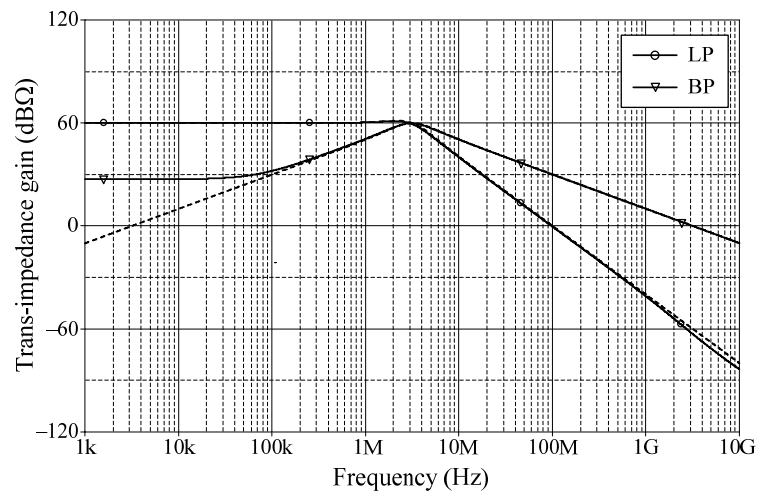
Figure 9. LP and BP frequency characteristics for TIM (simulated in solid line, theoretical in dashed line).

Table 3. Simulated f_o and corresponding percentage errors of the proposed mixed-mode universal biquad filter in Figure 3, where theoretical f_o = 3.18 MHz.

		LP	BP	HP	BS	AP
VM	f_o (MHz)	3.098	3.105	3.064	2.999	3.030
	Error (%)	2.579	2.371	3.638	5.686	4.714
CM	f_o (MHz)	3.099	3.106	3.068	2.964	3.010
	Error (%)	2.547	2.336	3.522	6.786	5.346
TAM	f_o (MHz)	3.100	3.104	3.067	2.964	3.009
	Error (%)	2.525	2.406	3.557	6.786	5.377
TIM	f_o (MHz)	3.100	3.106	—	—	—
	Error (%)	2.519	2.343	—	—	—
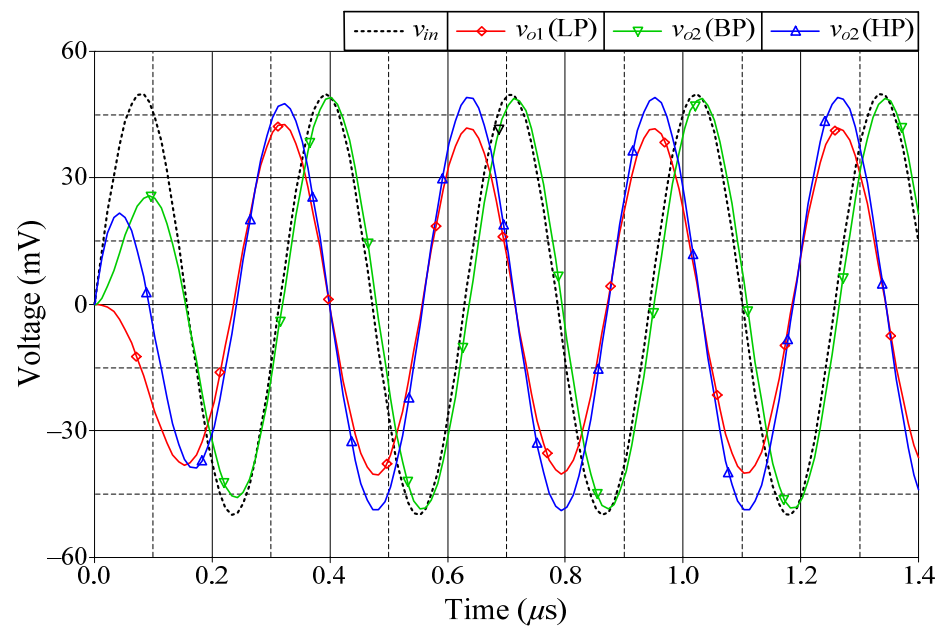
Figure 10. Time-domain responses of the LP, BP, and HP filters in VM.
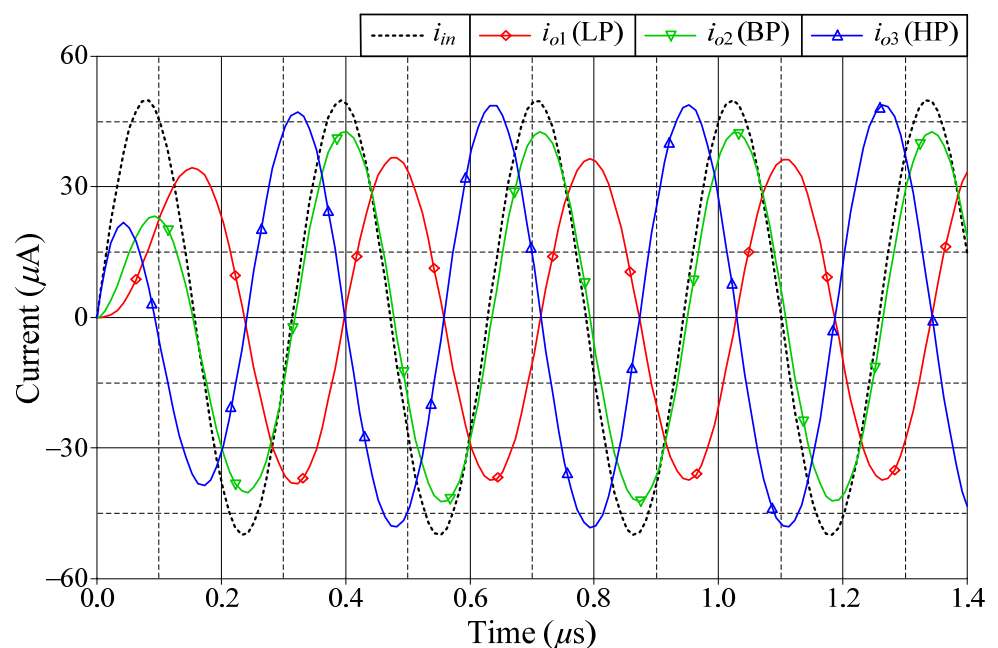
Figure 11. Time-domain responses of the LP, BP, and HP filters in CM.
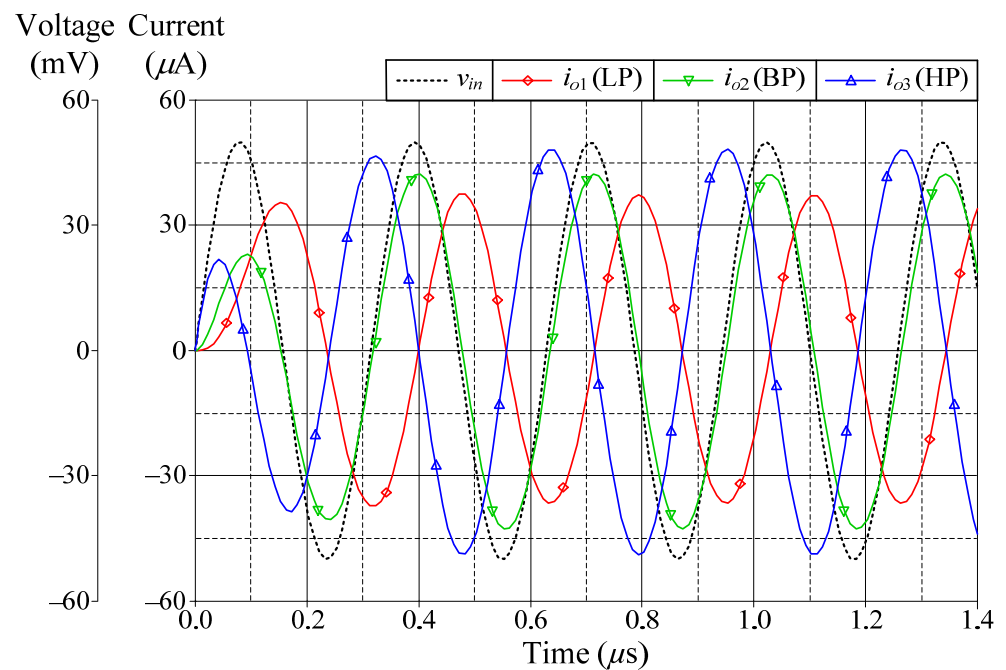
Figure 12. Time-domain responses of the LP, BP, and HP filters in TAM.
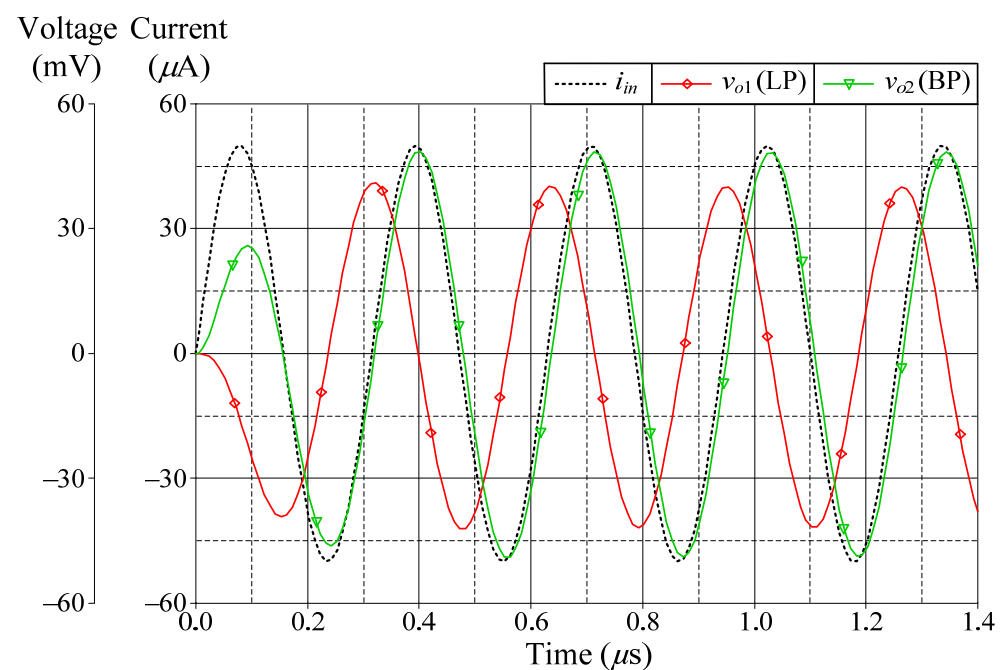
Figure 13. Time-domain responses of the LP and BP filters in TIM.

In addition, the orthogonal tunability of a high-Q value for a BP filter in VM is shown in Figure 14. The filter is designed to operate at f_o = 3.18 MHz with $g_{mA} = g_{mB} = g_{mC}$ = 1 mA/V. By simply adjusting the R value for 0.5 kΩ, 10 kΩ, and 50 kΩ, the BP responses with various Q values of 0.5, 10, and 50 are achieved, respectively. Based on the measured data, the Q value was evaluated as 0.495, 8.273, and 44.25, respectively. The relative variation of the Q factor remained less than 12%, even when Q reached 50.

Table 4. THDs and DC components of VM, CM, TAM, and TIM outputs with 3.18 MHz sinusoidal input signal.

		LP	BP	HP	BS	AP
VM	THD (%)	0.47	0.45	0.55	1.92	1.29
	DC component (mV)	9.55	2.36	2.37	2.46	3.04
CM	THD (%)	1.5	1.49	0.9	1.87	1.39
	DC component (μA)	10.79	4.42	0.044	10.74	15.17
TAM	THD (%)	1.57	1.45	0.9	1.86	1.26
	DC component (μA)	10.74	4.43	0.015	10.72	15.15
TIM	THD (%)	0.58	0.38	—	—	—
	DC component (mV)	9.62	2.39	—	—	—
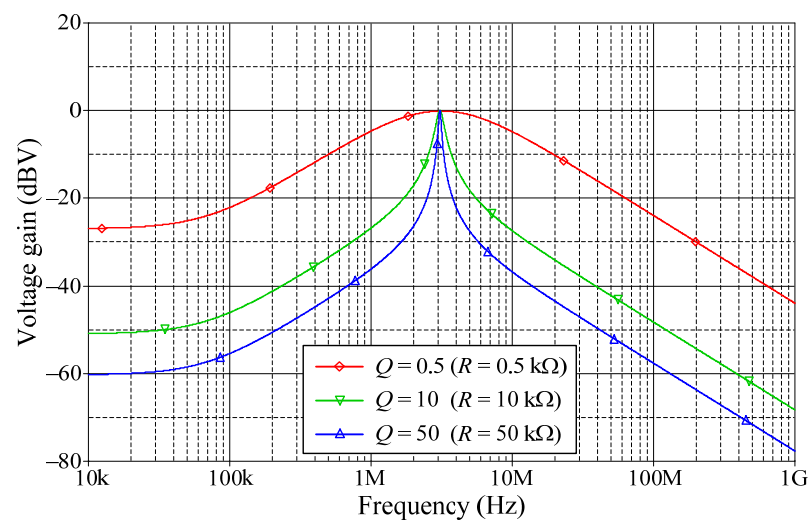
Figure 14. Tunability of Q with f_o unchanged for BP filter in VM.

The effect of temperature variation on the filter parameters is now being investigated. For this purpose, the proposed filter was simulated under ambient temperature changes ranging from 0 to 100 °C with a step of 25 °C. Figure 15 demonstrates the gain and phase variations of the AP filter in VM operation. The findings reveal that, for different temperatures, the gain and phase at f_o vary from −0.44 to −0.5 dBV and from −172 to −223°, respectively.
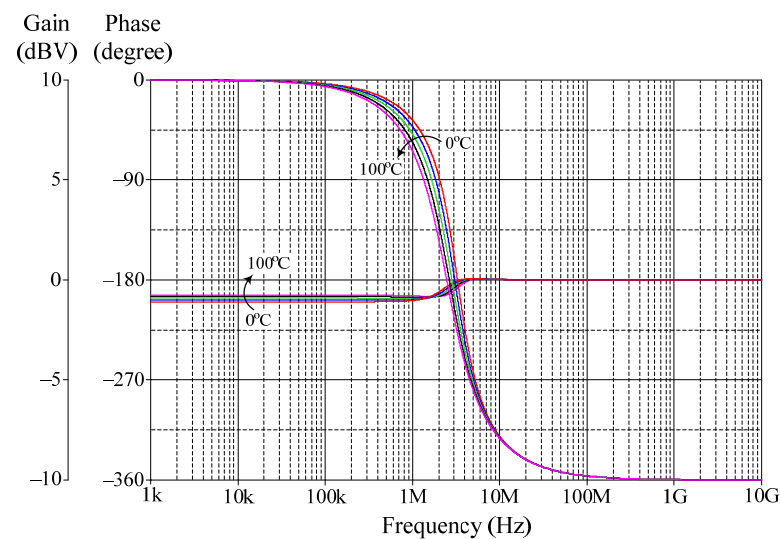
Figure 15. Frequency responses of AP filter in VM for different temperatures (0 °C, 25 °C, 50 °C, 75 °C, and 100 °C).

6.2. Simulation Verifications of the Proposed Dual-Mode Quadrature Oscillator

Based on previous component settings, the simulated quadrature voltages v_{osc1} and v_{osc2} of the proposed dual-mode quadrature oscillator in Figure 4 are displayed in Figure 16. Figure 16a shows the steady-state waveforms of v_{osc1} and v_{osc2}, whereas Figure 16b presents the frequency spectrums of the oscillation output voltages. As per the findings, the simulated f_{osc} was found to be 2.76 MHz, and the phase shift between v_{osc1} and v_{osc2} was 85.76°. The attenuations at the second harmonic for v_{osc1} and v_{osc2} were 30.30 dBm and 31.45 dBm, respectively. Further, the percentage of THD was 2.46% for v_{osc1} and 4.28% for v_{osc2}.

(a)

(b)
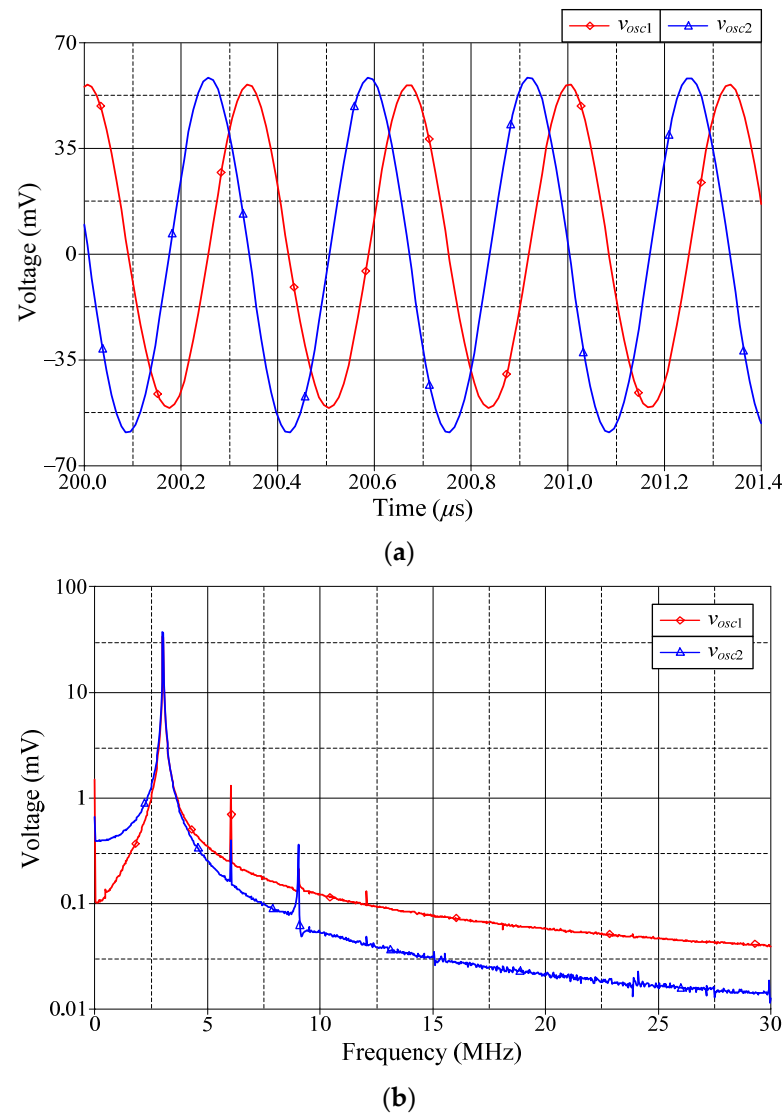
Figure 16. Quadrature output voltages v_{osc1} and v_{osc2}: (**a**) steady-state waveforms; (**b**) frequency spectrums.

Similarly, the simulated steady-state responses and the corresponding frequency spectrums of i_{osc1}, i_{osc2}, and i_{osc3} are also given in Figure 17. The phase shifts between i_{osc1} and i_{osc2}, and i_{osc1} and i_{osc3} were measured to be 92.73° and 177.82°, respectively. The second-harmonic attenuations for i_{osc1}, i_{osc2}, and i_{osc3} were 30.05 dBµ, 30.88 dBµ, and 30.87 dBµ, respectively, while the percentage THDs of i_{osc1}, i_{osc2}, and i_{osc3} were 3.86%, 4.16%, and 3.50%, respectively.
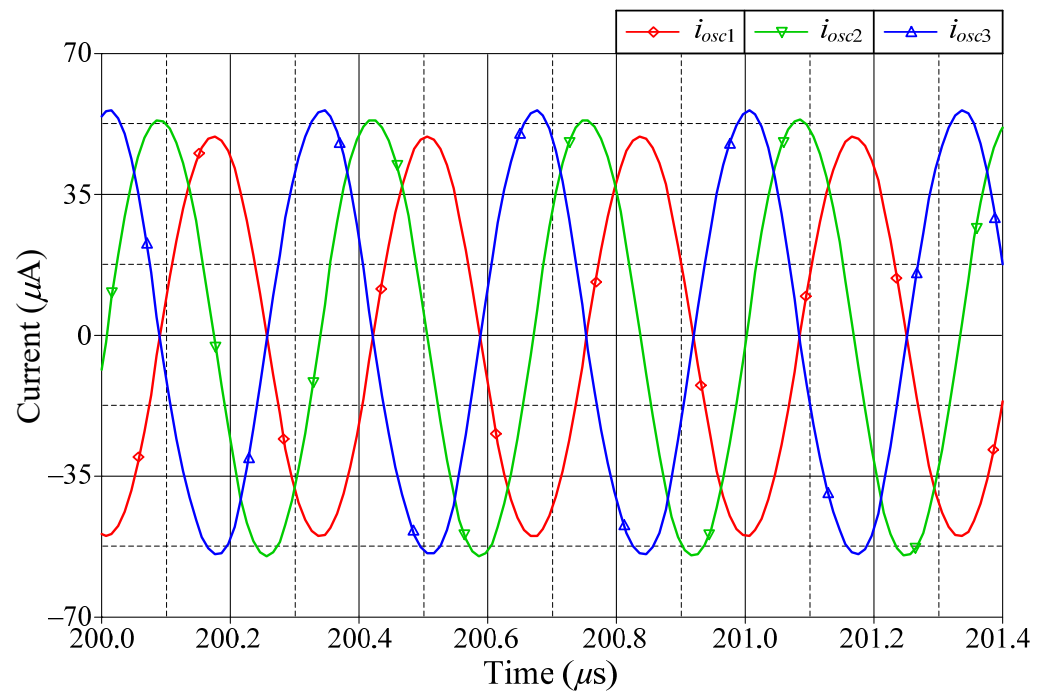
(**a**)
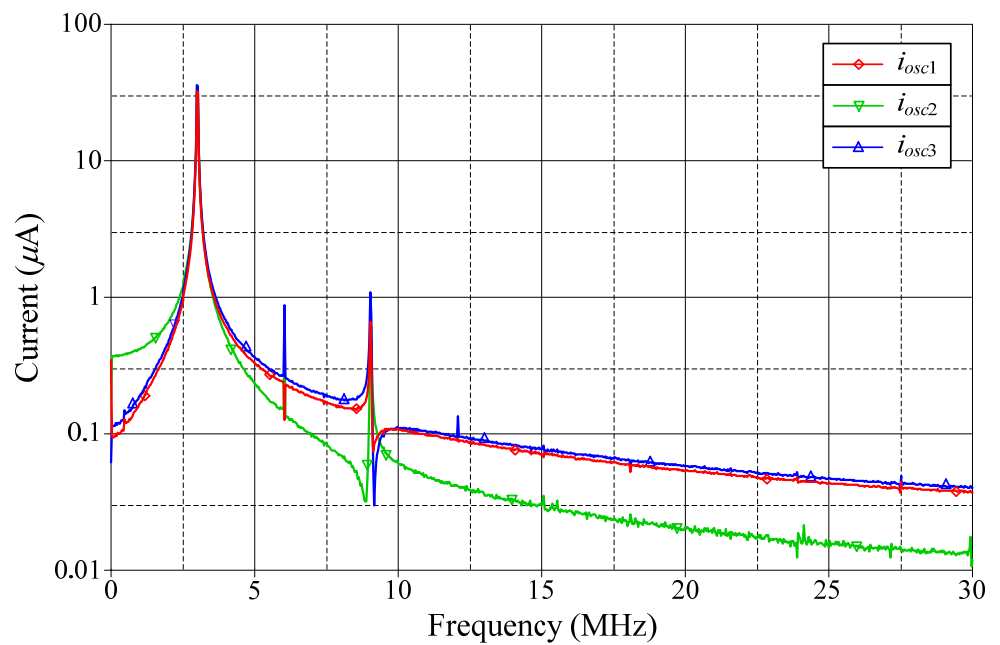
(**b**)

Figure 17. Simulated quadrature output currents i_{osc1}, i_{osc2}, and i_{osc3}: (**a**) steady-state waveforms; (**b**) frequency spectrums.

Due to the VDGA transconductance gain g_{mk} is tuned by the bias current I_{Bk}, the f_{osc} of the proposed circuit is a current tunable function. Figure 18 demonstrates the calculation and simulation results for the variations of f_{osc} as a function of I_B, where $I_B = I_{BA} = I_{BB} = I_{BC}$.
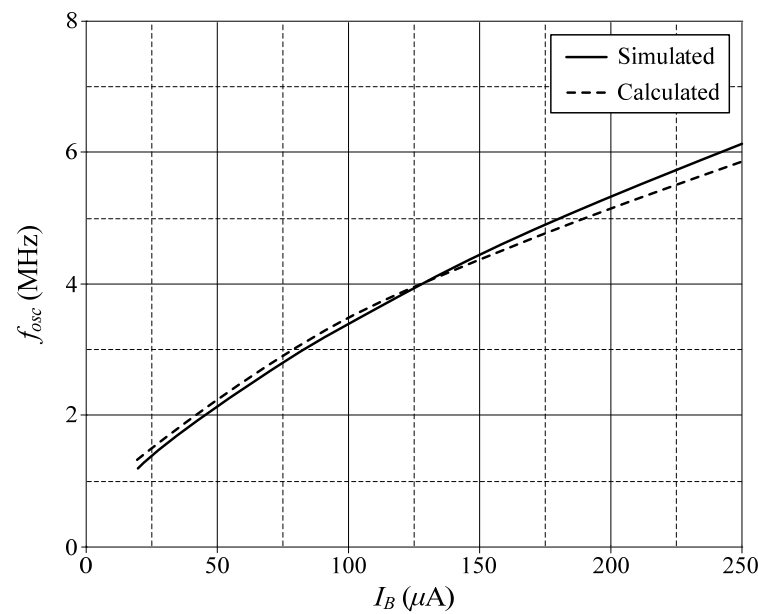
Figure 18. Variations of f_{osc} against I_B for the proposed quadrature oscillator in Figure 4.

7. Experimental Results

7.1. Experimental Verifications of the Proposed Mixed-Mode Universal Filter

To further support the theory, the suggested circuits in Figures 3 and 4 were experimentally verified. As shown in Figure 19, the VDGA was built-in hardware utilizing off-the-shelf IC dual-OTA LM13600s from National Semiconductor [58]. To bias the LM13600, DC supply voltages of ±5 V were employed. A prototype hardware setup for verification purposes of the proposed circuit is illustrated in Figure 20. The component values were set as follows: $g_{mA} = g_{mB} = g_{mC} = 1$ mA/V ($I_{BA} = I_{BB} = I_{BC} = 50$ μA), $R = 1$ kΩ, and $C_1 = C_2 = 680$ pF, actually results in $f_o = 234$ kHz, and $Q = 1$. In order to measure the input signals for the CM and TIM, a voltage-to-current converter with IC AD844 [59] and a converting resistor R_C of 1 kΩ was used, as illustrated in Figure 21. In Figure 22, two extra AD844s and R_C were used as a current-to-voltage conversion for output signal measurements in CM and TAM operations.
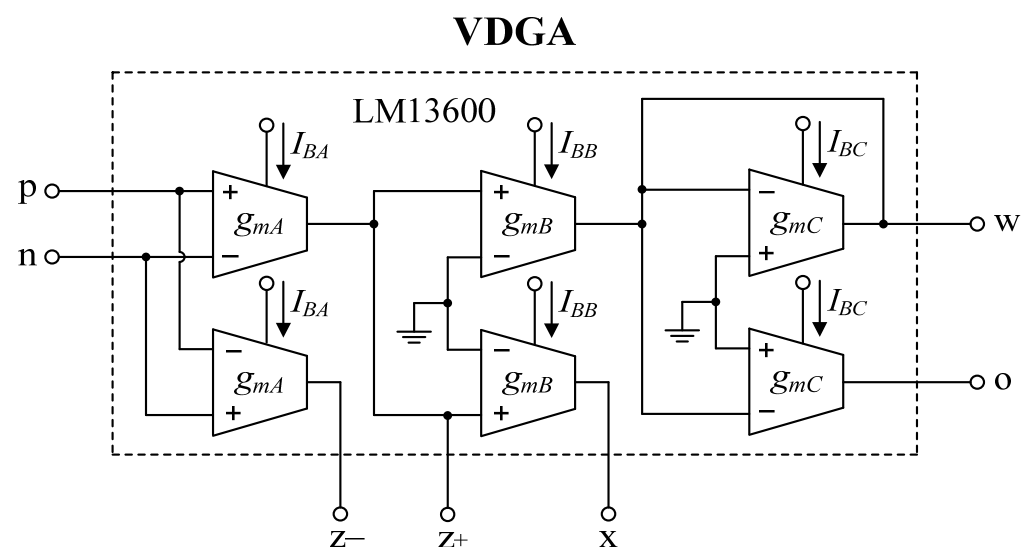
VDGA

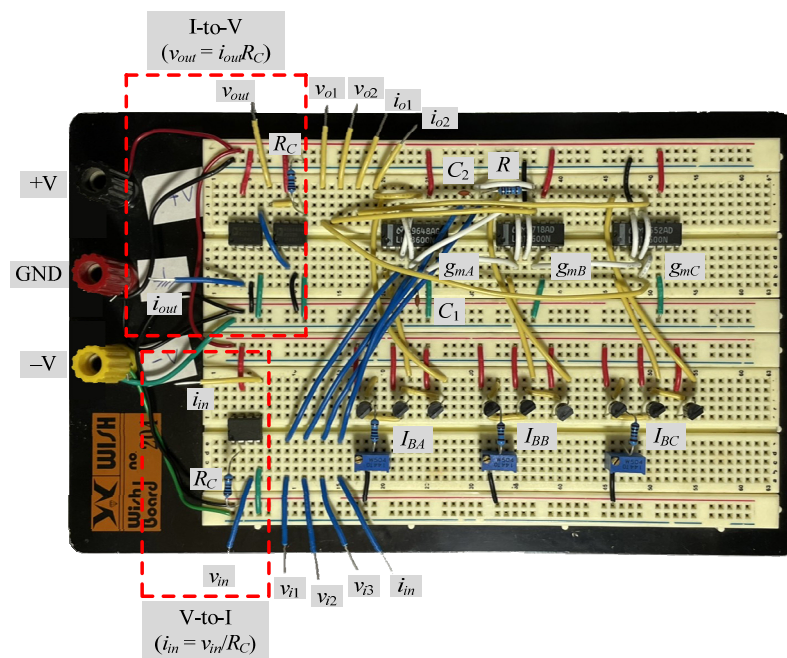**Figure 19.** Practical VDGA implementation using off-the-shelf IC LM13600s.

Figure 20. Prototype hardware setup for the experimental verification.
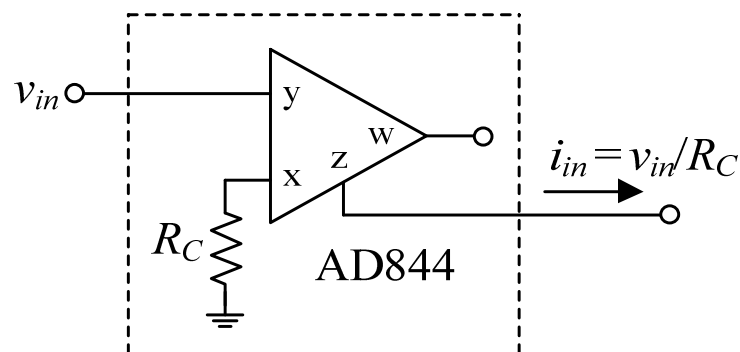

Figure 21. Voltage-to-current conversion for CM and TIM input signal measurements.
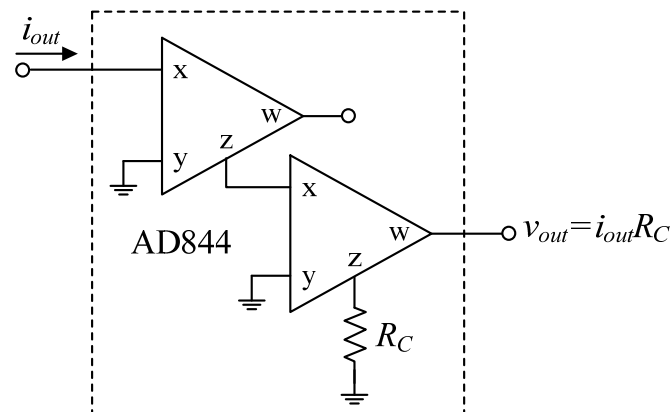

Figure 22. Current-to-voltage conversion for CM and TAM output signal measurements.

Figures 23–27 show the measurements of the input and output waveforms and the relevant output spectrums for the proposed VM filter with a 20 mV (peak) sinewave input voltage at 234 kHz. The THD values of the LP, BP, HP, BS, and AP output responses were 1.88%, 0.25%, 0.57%, 1.84%, and 2.66%, respectively. As can be seen from Figures 23b, 24b, 25b, 26b and 27b, the spurious-free dynamic range (SFDR) for the cases of LP, BP, HP, BS, and AP were measured at 35.03 dBc, 52.65 dBc, 45.68 dBc, 36.35 dBc, and 34.33 dBc, respectively. Figure 28 also shows the experimental gain-frequency responses of the proposed VM filter. The measured results of f_0 of VM, CM, TAM, and TIM were found to be 241.13 kHz (error ~+3%), 227.08 kHz (error ~−2.98%), 227.38 kHz (error ~−2.87%), and 233.32 kHz (error ~−0.33%), respectively. In all cases, the practically observed behavior of the circuit was found to be consistent with the theoretical predictions. The experimental test results, thus, verify the practicability of the suggested design. Nevertheless, one observes that the discrepancy between the theoretical and measured results was originally caused by non-ideal gain and parasitic impedance effects of the LM13600s and AD844s. The stray capacitances generated by the breadboard circuit realization also affect the frequency performance of the circuit in experimental testing.
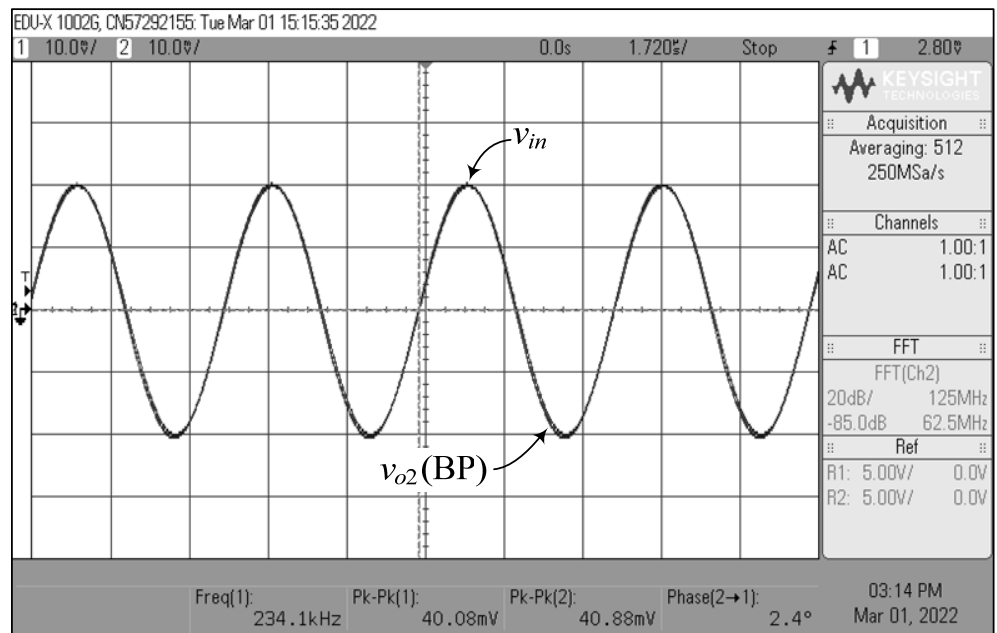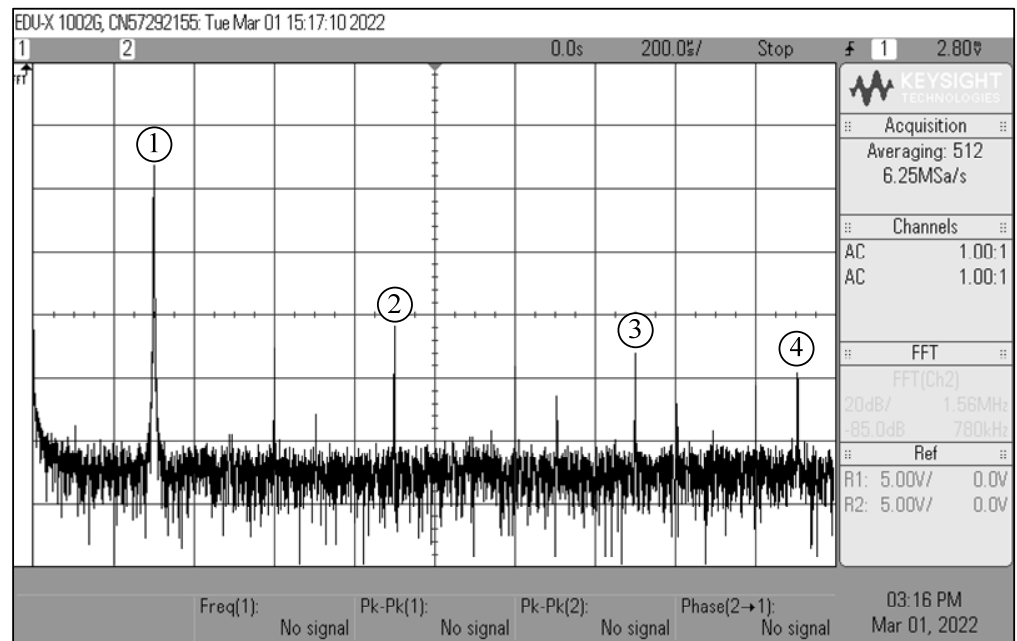

(**a**)
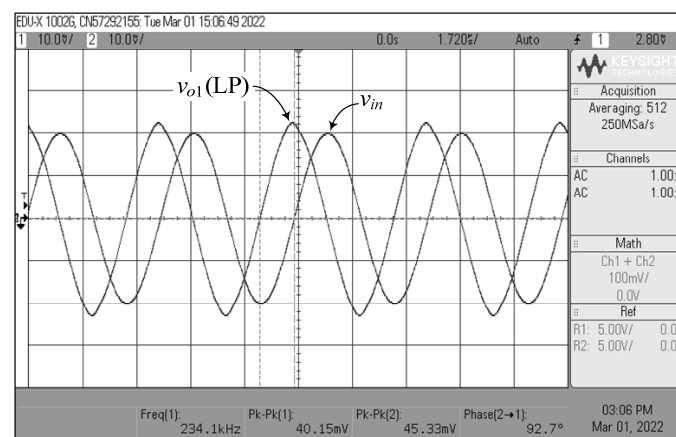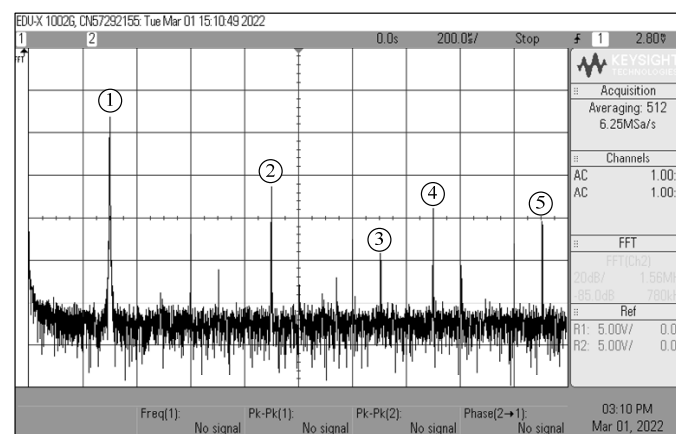
No.	Frequency (kHz)	Gain (dBV)
1	234.05	−37.95
2	702	−72.98
3	1017.90	−103.49
4	1170.78	−82.34
5	1486.68	−90.60

(**b**)

Figure 23. Measured waveforms of the LP filter in VM: (**a**) input and output time responses; (**b**) frequency spectrum.

(**a**)

No.	Frequency (kHz)	Gain (dBV)
1	234.05	−38.50
2	702	−91.15
3	1170.78	−98.67
4	1486.68	−107.58

(**b**)

Figure 24. Measured waveforms of the BP filter in VM: (**a**) input and output time responses; (**b**) frequency spectrum.

(**a**)
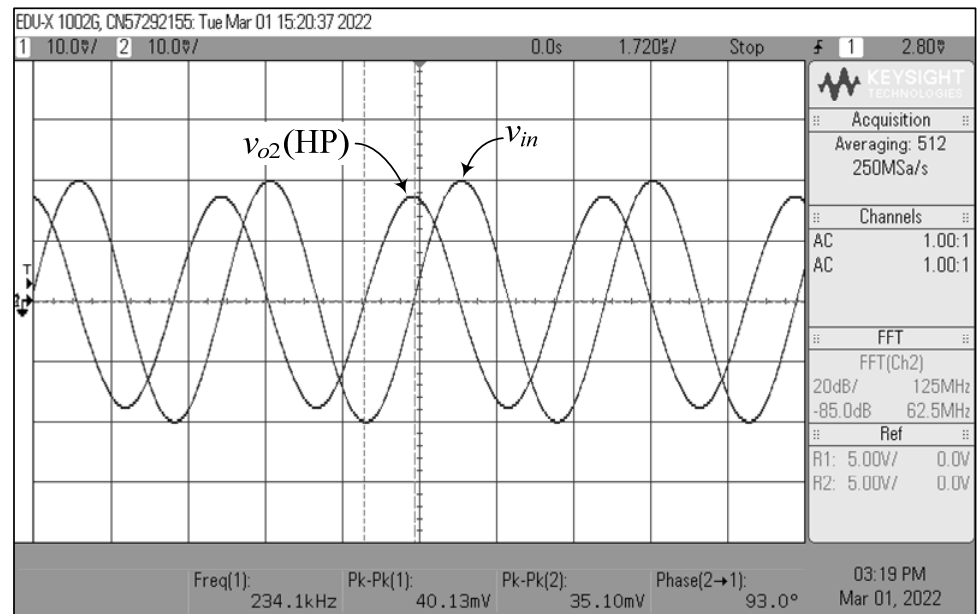
No.	Frequency (kHz)	Gain (dBV)
1	234.05	−39.86
2	702	−85.54
3	1170.78	−92.20
4	1486.68	−108.52

(**b**)

Figure 25. Measured waveforms of the HP filter in VM: (**a**) input and output time responses; (**b**) frequency spectrum.
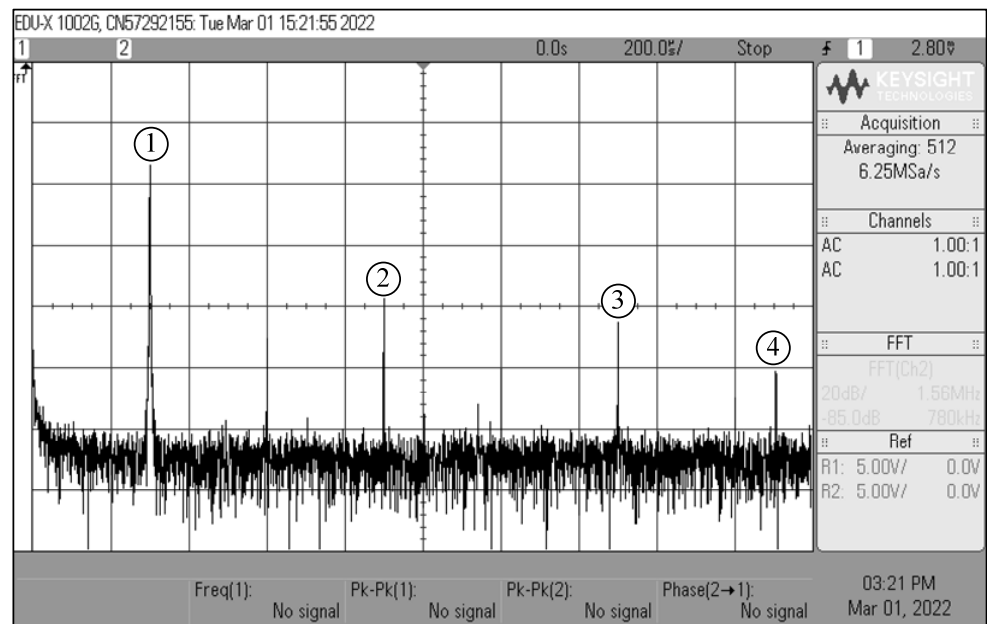
(**a**)
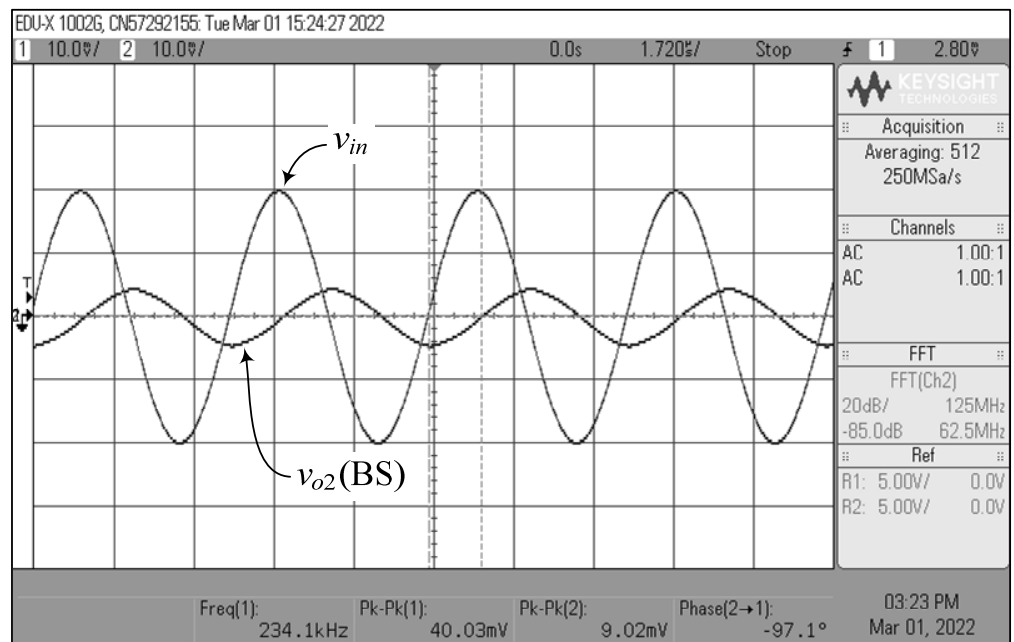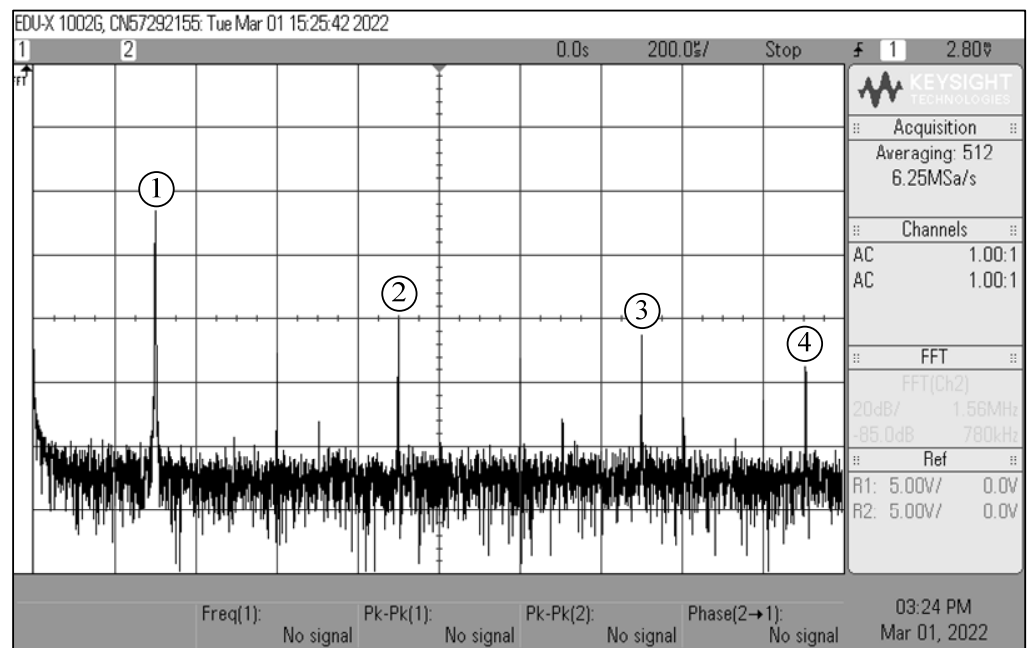
No.	Frequency (kHz)	Gain (dBV)
1	234.05	−52.05
2	702	−88.40
3	1170.78	−91.93
4	1486.68	−104.60

(**b**)

Figure 26. Measured waveforms of the BS filter in VM: (**a**) input and output time responses; (**b**) frequency spectrum.

(**a**)
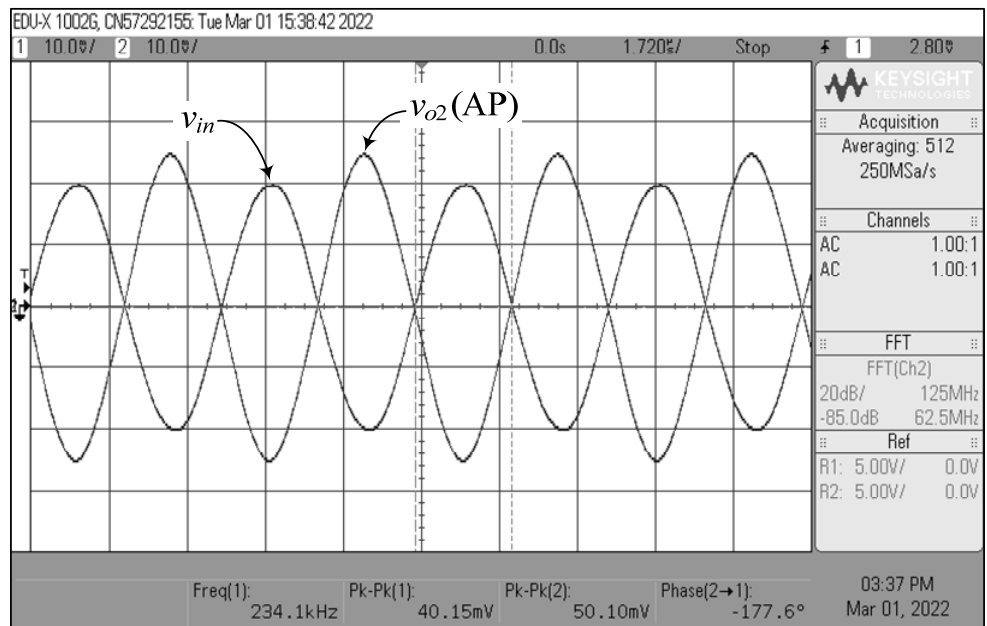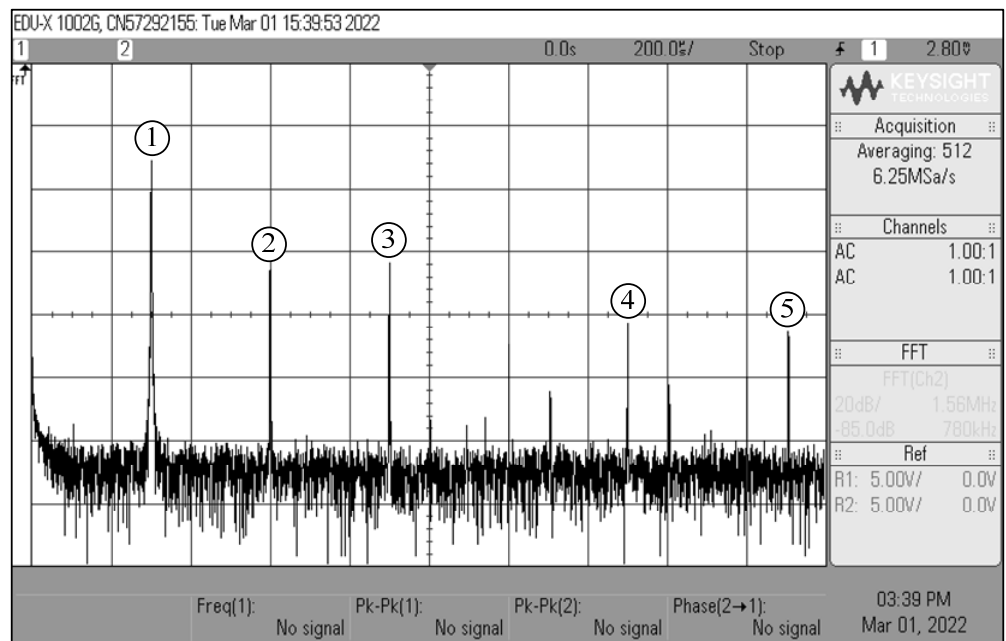
No.	Frequency (kHz)	Gain (dBV)
1	234.05	−36.99
2	468	−71.77
3	702	−71.32
4	1170.78	−89.43
5	1486.68	−94.55

(**b**)

Figure 27. Measured waveforms of the AP filter in VM: (**a**) input and output time responses; (**b**) frequency spectrum.
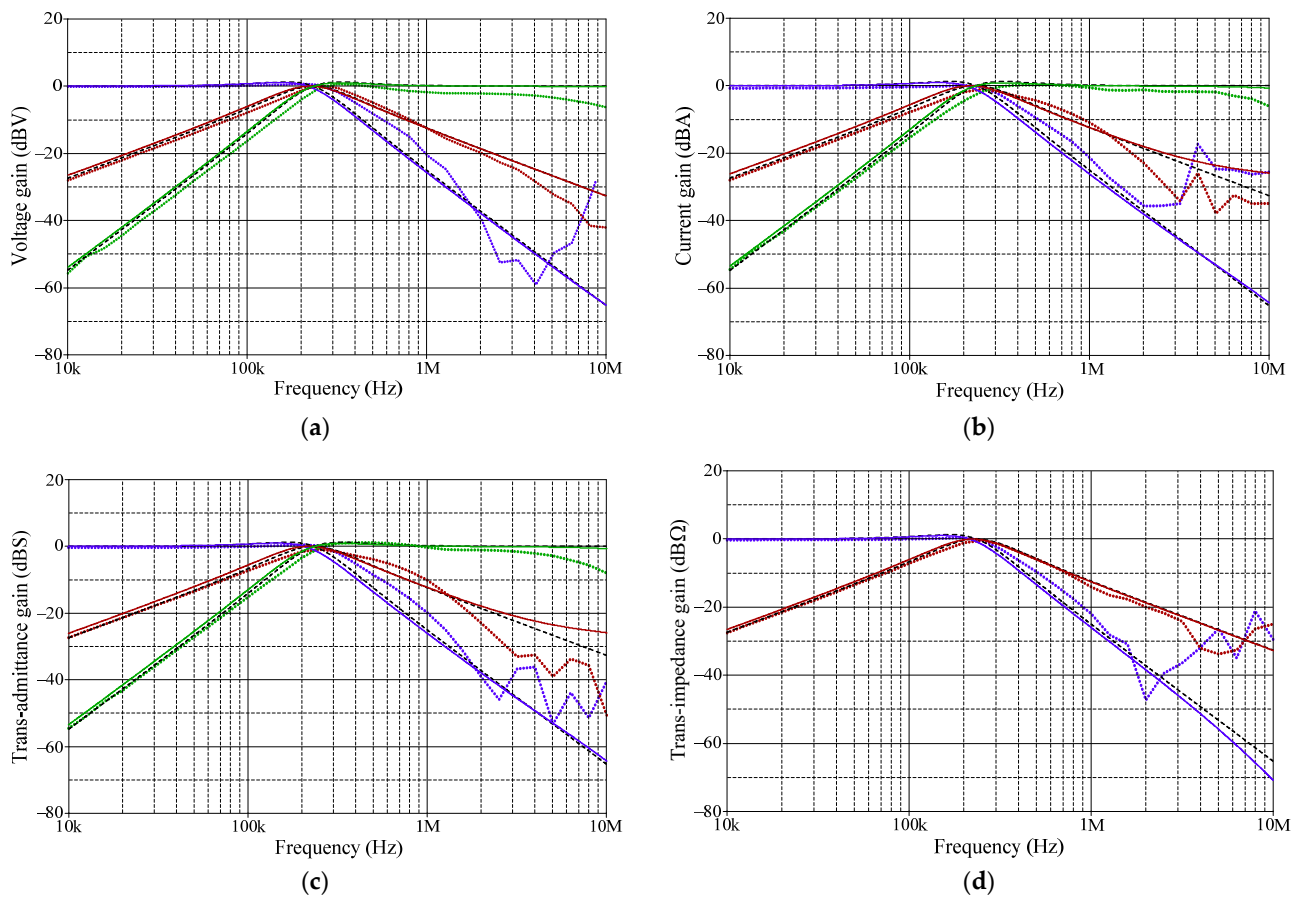
Figure 28. Measured and theoretical frequency responses of the proposed filter (measured in solid line, theoretical in dashed line, simulated in dotted lines): (**a**) LP, BP, and HP responses in VM; (**b**) LP, BP, and HP responses in CM; (**c**) LP, BP, and HP responses in TAM; (**d**) LP and BP responses in TIM.

7.2. Experimental Verifications of the Proposed Dual-Mode Quadrature Oscillator

According to the experimental measurements for the proposed dual-mode quadrature oscillator in Figure 4, the oscilloscope output waveforms in time-domain and Lissajous pattern of v_{osc1} and v_{osc2} are given in Figure 29. By using the same component values as in the previous filter case, the oscillator was constructed to oscillate at an OF of f_{osc} = 234 kHz. The f_{osc} observed was 234.1 kHz, which is extremely close to the theoretical value. The phase angle difference between v_{osc1} and v_{osc2} was roughly 95.1°, resulting in an absolute phase deviation of 5.67%. Figure 30 also shows the measured frequency spectrum of the v_{osc1} output. From the experimental testing, the THD and SFDR values for the output v_{osc1} were 2.85% and 31.38 dBc, respectively.

For i_{osc1}, i_{osc2}, and i_{osc3} measurements, the current-to-voltage converter circuit as shown in Figure 22 was also employed. The time-domain waveforms and the corresponding Lissajous figures of the oscillator output currents i_{osc1} and i_{osc2}, and i_{osc2} and i_{osc3} are illustrated in Figures 31 and 32, respectively. The quadrature-phase shifts between i_{osc1} and i_{osc2}, and i_{osc2} and i_{osc3} were 96.1° and 85.3°, respectively, deviating from the calculations by 6.78% and 5.22%. The frequency spectrum of the i_{osc1} output was also recorded and exhibited in Figure 33, with percentage THD and SFDR values of 2.05% and 34 dBc, respectively. Clearly, the generated waveforms observed in the experimental data validate the quadrature relationship of the suggested quadrature oscillator in both VM and CM.

Figure 29. Measured quadrature output voltages v_{osc1} and v_{osc2} of Figure 4: (**a**) time-domain waveforms; (**b**) Lissajous pattern.

No.	Frequency (kHz)	Gain (dBV)
1	234.05	−33.53
2	702	−64.91
3	1016.34	−90.49
4	1170.78	−74.95
5	1250.34	−95.98
6	1405.56	−94.30
7	1486.68	−83.95

Figure 30. Measured frequency spectrum of v_{osc1} output.
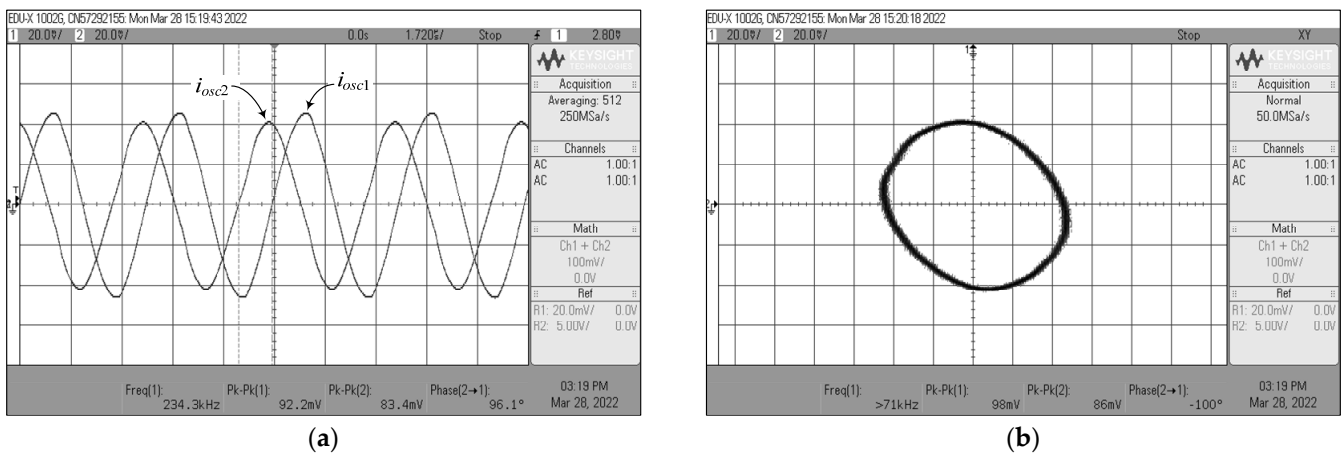
Figure 31. Measured quadrature output currents i_{osc1} and i_{osc2} of Figure 4: (**a**) time-domain waveforms; (**b**) Lissajous pattern.
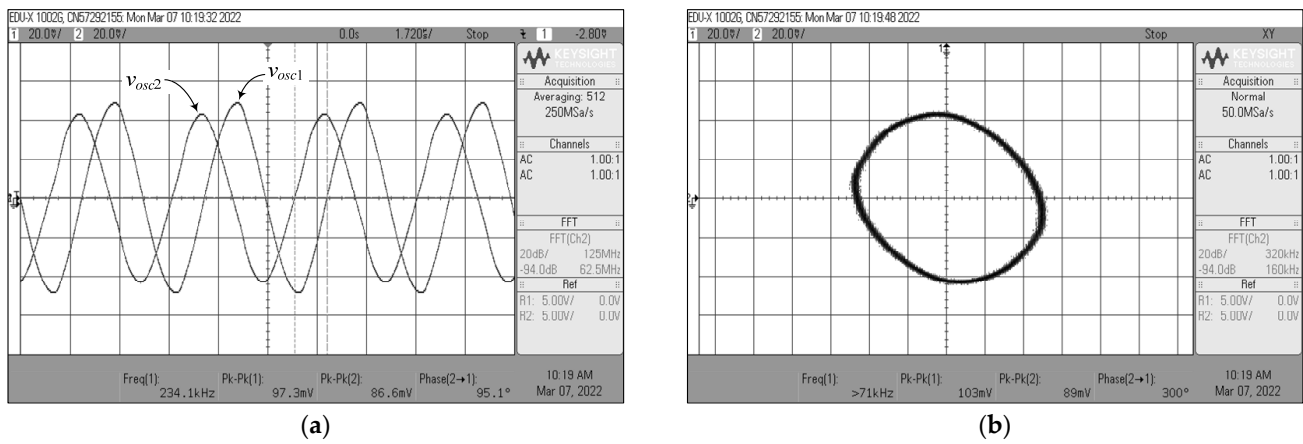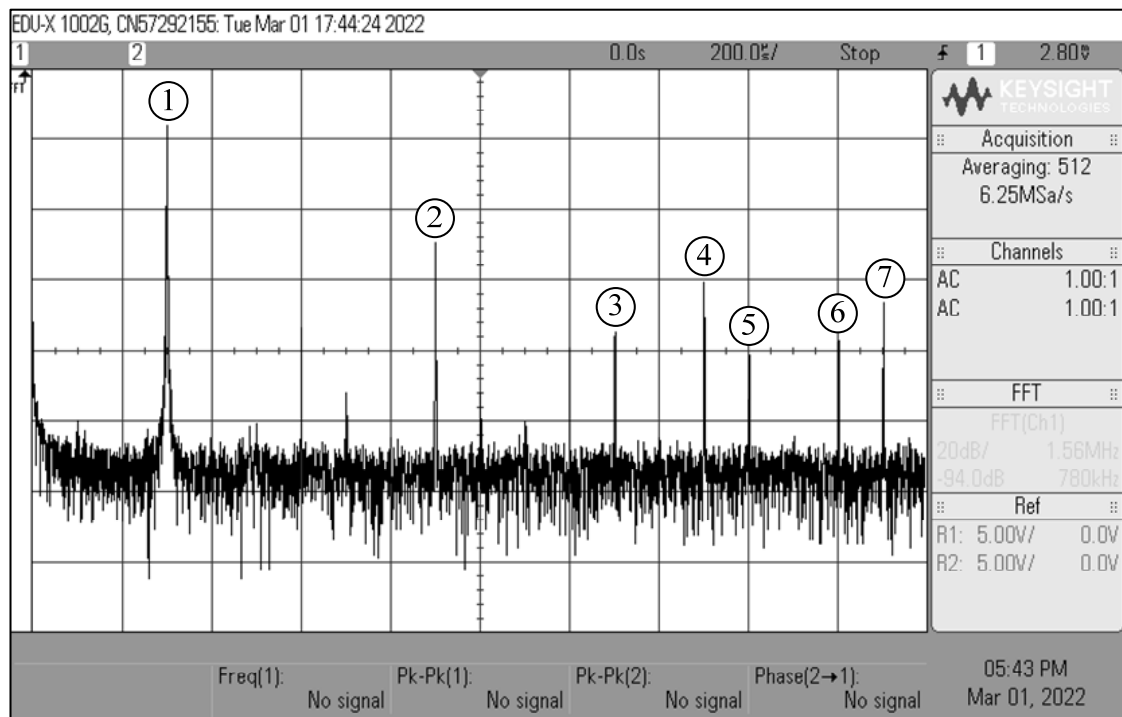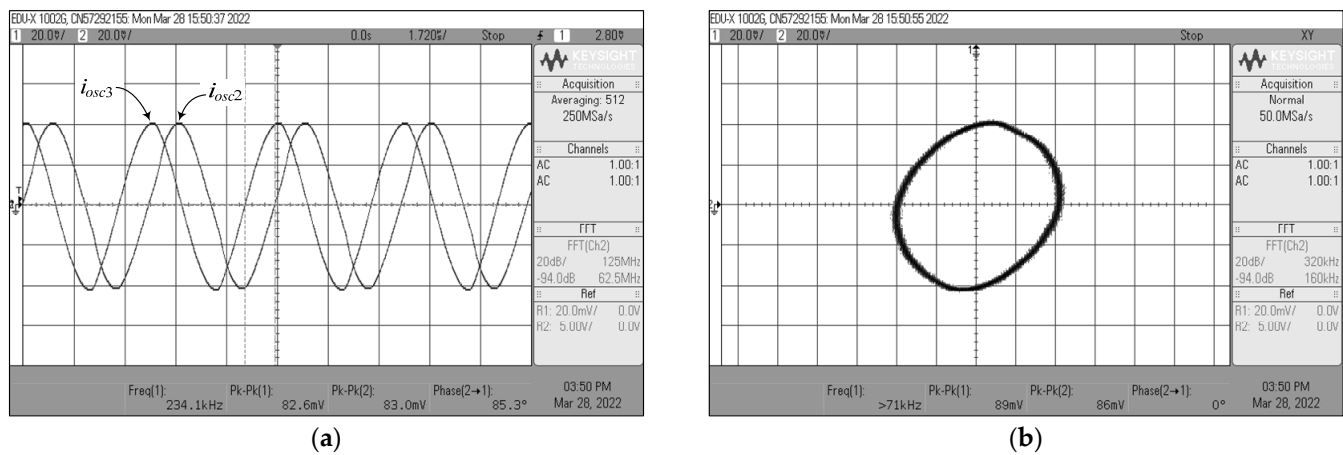

Figure 32. Measured quadrature output currents i_{osc2} and i_{osc3} of Figure 4: (**a**) time-domain waveforms; (**b**) Lissajous pattern.
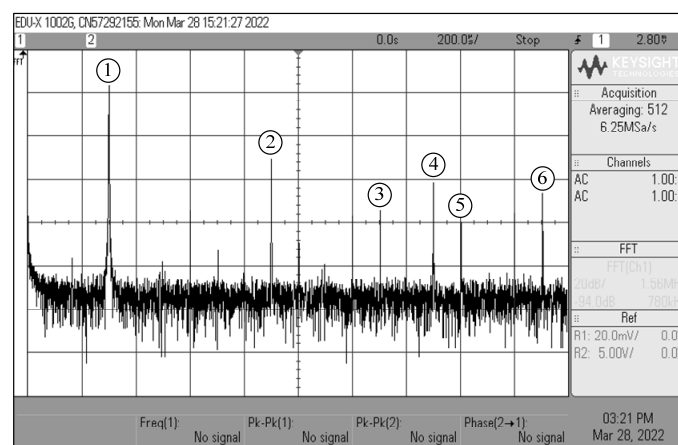
No.	Frequency (kHz)	Gain (dBV)
1	234.05	−32.15
2	702	−66.10
3	1016.34	−91.57
4	1170.78	−75.68
5	1250.34	−96.24
6	1486.68	−81.48

Figure 33. Measured frequency spectrum of i_{osc1} output.

8. Discussion

At this point, we would like to briefly discuss the superiority of the proposed MUBF and DMQO design over similar existing designs in the literature. The following observations are based on Table 1.

In contrast to the topologies in [1–40], the proposed circuit uses the same topology to perform both MUBF and DMQO, whereas the works referenced only perform MUBF [1–31] or DMQO [32–40]. With regard to the MUBF topologies introduced in [5,7,9,10,12–15,18,22,23,25–27,30], all five biquadratic filter functions are implemented in all four modes of operation. These circuits, however, employ more active components, especially at least two active components, than the suggested circuit. Some have three or more passive components [9,12–15,22–31] or DMQO [32,33]. In addition to the filters of [2,6,8,11,16,19,20,24], they are limited to only two modes of operation. Designing with a low component count is a simple technique to reduce the total power consumption of the designed circuit. Even though compact MUBF circuits implemented with a single active element have been proposed in [3,8,16,21,24,27,28,41,48], these biquads still use more passive elements than the MUBF circuit proposed in this work. While the designs described in [4,7,12,14,15,18–20,23,26,45,49,50] are interesting, they suffer from the usage of two or more different types of active components, which complicates circuit implementation.

In the QO configurations [47,48], there are floating passive elements that are not encouraged for further integration. Several QO designs operated in either VM [44,47,49] or CM [42,43]. As compared to the proposed DMQO circuit, it not only uses grounded passive elements, but it also provides both voltage and current quadrature outputs simultaneously.

The topologies in [1,2,6–8,10,13,18,21,23,28,31,40,42,43,48,50] do not offer independent adjustment of their important parameters, but even the proposed MUBF and DMQO design allows independent parameter modification through transconductance (g_m) or single resistance value. Also in the existing literature [2–4,6,8,9,12,13,19,22,23,31,32,34,39,47], an electronic control of various parameters is not available.

As a conclusion, it should be noted that the proposed MUBF and DMQO circuit in this study is capable of fulfilling all of the performance features described above simultaneously and without trade-offs.

9. Conclusions

This work proposes a compact mixed-mode universal biquadratic filter and dual-mode quadrature oscillator circuit using a single voltage differencing gain amplifier (VDGA). In this design, a canonical structure with one resistor and two capacitors is employed. The proposed universal biquad filter is able to realize generic second-order filter functions in all four modes of operation, namely, VM, CM, TAM, and TIM. It has the feature of orthogonal control of ω_o and Q characteristics, and simultaneously the ability to implement a high-Q filter with a single resistance adjustment. The quadrature oscillator, which generates both voltage and current output signals simultaneously, is also feasible by slight modification of the proposed configuration. Both the oscillation condition and the oscillation frequency of the proposed quadrature oscillator are non-interactively controlled. The circuits are subjected to non-ideal analysis, including tracking error and parasitic element effects. The simulation and experimental findings prove that the suggested circuit performs in both the mixed-mode universal biquad filter and the dual-mode quadrature oscillator.

Author Contributions: Conceptualization, N.R. and W.T.; methodology, N.R. and W.T.; software, N.R. and T.P.; validation, N.R., W.T., and T.P.; formal analysis, N.R. and W.T.; investigation, N.R., W.T. and T.P.; resources, N.R. and W.T.; data curation, N.R., W.T. and T.P.; writing—original draft preparation, W.T.; writing—review and editing, W.T.; visualization, W.T. and T.P.; supervision, W.T.; project administration, W.T.; funding acquisition, N.R., W.T. and T.P. All authors have read and agreed to the published version of the manuscript.

Institutional Review Board Statement: Not applicable.

Symbols and Nomenclatures: The following symbols and nomenclatures are used in this manuscript:

VDGA	voltage differencing gain amplifier
VM	voltage-mode
CM	current-mode
TAM	trans-admittance-mode
TIM	trans-impedance-mode
LP	low-pass
BP	band-pass
HP	high-pass
BS	band-stop
AP	all-pass
MUBF	mixed-mode universal biquadratic filter
QO	quadrature oscillator
DMQO	dual-mode QO
OC	oscillation condition
OF	oscillation frequency
g_m	transconductance gain of the VDGA
β	voltage transfer gain of the VDGA
μ	effective channel electronic mobility
C_{ox}	gate-oxide capacitance per unit area
W	effective channel width
L	effective channel length
T_V	transfer function of voltage-mode filter
T_I	transfer function of current-mode filter
T_Y	transfer function of trans-admittance-mode filter
T_Z	transfer function of trans-impedance-mode filter
ω_o	natural angular frequency of biquadratic filter
f_o	natural frequency of biquadratic filter
Q	quality factor of biquadratic filter
ω_{osc}	natural angular frequency of oscillator
f_{osc}	frequency of oscillator
$e^{j90°}$	Euler's formula shows a 90° phase difference between two signals
$e^{j180°}$	Euler's formula shows a 180° phase difference between two signals
α	non-ideal transconductance gain
δ	non-ideal voltage transfer gain
ε_α	tracking error of transconductance gain
ε_δ	tracking error of voltage transfer gain
dBV	voltage decibel
dBA	ampere decibel
dBS	siemens decibel
dBΩ	Ohm decibel
dBm	mili decibel
dBμ	micro decibel
dBc	decibels relative to the carrier
THD	total harmonic distortion
SFDR	spurious-free dynamic range

References

1. Abuelma'atti, M.T. A novel mixed-mode current-controlled current-conveyor-based filter. *Act. Passiv. Electron. Compon.* **2003**, *26*, 185–191. [CrossRef]
2. Gupta, S.S.; Senani, R. New voltage-mode/current-mode universal biquad filter using unity-gain cells. *Int. J. Electron.* **2006**, *93*, 769–775. [CrossRef]
3. Lee, C.N.; Chang, C.M. Single FDCCII-based mixed-mode biquad filter with eight outputs. *AEU—Int. J. Electron. Commun.* **2009**, *63*, 736–742. [CrossRef]
4. Minaei, S.; Ibrahim, M.A. A mixed-mode KHN-biquad using DVCC and grounded passive elements suitable for direct cascading. *Int. J. Circuit Theory Appl.* **2009**, *37*, 793–810. [CrossRef]
5. Chen, H.P.; Liao, Y.Z.; Lee, W.T. Tunable mixed-mode OTA-C universal filter. *Analog Integr. Circuits Signal Process.* **2009**, *58*, 135–141. [CrossRef]
6. Horng, J.W. High-order current-mode and transimpedance-mode universal filters with multiple-inputs and two-outputs using MOCCIIs. *Radioengineering* **2009**, *18*, 537–543.
7. Lee, C.N. Multiple-mode OTA-C universal biquad filters. *Circuits Syst. Signal Process.* **2010**, *29*, 263–274. [CrossRef]
8. Yuce, E. Fully integrable mixed-mode universal biquad with specific application of the CFOA. *AEU—Int. J. Electron. Commun.* **2010**, *64*, 304–309. [CrossRef]
9. Liao, W.B.; Gu, J.C. SIMO type universal mixed-mode biquadratic filter. *Indian J. Eng. Mater. Sci.* **2011**, *18*, 443–448.
10. Pandey, N.; Paul, S.K. Mixed mode universal filter. *J. Circuits Syst. Comput.* **2013**, *22*, 1250064. [CrossRef]
11. Yeşil, A.; Kaçar, F. Electronically tunable resistorless mixed mode biquad filters. *Radioengineering* **2013**, *22*, 1016–1025.
12. Lee, C.N. Independently tunable mixed-mode universal biquad filter with versatile input/output functions. *AEU—Int. J. Electron. Commun.* **2016**, *70*, 1006–1019. [CrossRef]
13. Lee, C.N. Mixed-mode universal biquadratic filter with no need of matching conditions. *J. Circuits Syst. Comput.* **2016**, *25*, 1650106. [CrossRef]
14. Singh, D.; Afzal, N. Fully digitally programmable generalized mixed mode universal filter configuration. *Circuits Syst. Signal Process.* **2016**, *35*, 1457–1480. [CrossRef]
15. Singh, D.; Afzal, N. Digitally programmable mixed mode universal filter using followers-a minimal realization. *Analog Integr. Circuits Signal Process.* **2016**, *86*, 289–298. [CrossRef]
16. Pandey, R.; Pandey, N.; Singhal, N. Single VDTA based dual mode single input multioutput biquad filter. *J. Eng.* **2016**, *2016*, 1674343. [CrossRef]
17. Chen, H.P.; Yang, W.S. Electronically tunable current controlled current conveyor transconductance amplifier-based mixed-mode biquadratic filter with resistorless and grounded capacitors. *Appl. Sci.* **2017**, *7*, 244. [CrossRef]
18. Parvizi, M.; Taghizadeh, A.; Mahmoodian, H.; Kozehkanani, Z.D. A low-power mixed-mode SIMO universal G_m–C filter. *J. Circuits Syst. Comput.* **2017**, *26*, 1750164. [CrossRef]
19. Horng, J.W.; Wu, C.M.; Herencsar, N. Current-mode and transimpedance-mode universal biquadratic filter using two current conveyors. *Indian J. Eng. Mater. Sci.* **2017**, *24*, 461–468.
20. Cini, U.; Aktan, M. Dual-mode OTA based biquadratic filter suitable for current-mode applications. *AEU—Int. J. Electron. Commun.* **2017**, *80*, 43–47. [CrossRef]
21. Faseehuddin, M.; Sampe, J.; Shireen, S.; Ali, S.H.M. A novel mix-mode universal filter employing a single active element and minimum number of passive components. *Inf. MIDEM* **2017**, *47*, 211–221.
22. Chaturvedi, B.; Mohan, J.; Kumar, A. A new versatile universal biquad configuration for emerging signal processing applications. *J. Circuits Syst. Comput.* **2018**, *27*, 1850196. [CrossRef]
23. Safari, L.; Barile, G.; Ferri, G.; Stornelli, V. A new low-voltage low-power dual-mode VCII-based SIMO universal filter. *Electronics* **2019**, *8*, 765. [CrossRef]
24. Albrni, M.A.; Faseehuddin, M.; Sampe, J.; Ali, S.H.M. Novel dual mode multifunction filter employing highly versatile VD-DXCC. *Inf. MIDEM* **2019**, *49*, 169–176. [CrossRef]
25. Bhaskar, D.R.; Raj, A.; Kumar, P. Mixed-mode universal biquad filter using OTAs. *J. Circuits Syst. Comput.* **2020**, *29*, 2050162. [CrossRef]
26. Albrni, M.I.A.; Mohammad, F.; Herencsar, N.; Sampe, J.; Ali, S.H.M. Novel electronically tunable biquadratic mixed-mode universal filter capable of operating in MISO and SIMO configurations. *Inf. MIDEM* **2020**, *50*, 189–203. [CrossRef]
27. Mohammad, F.; Herencsar, N.; Albrni, M.A.; Sampe, J. Electronically tunable mixed mode universal filter employing a single active block and a minimum number of passive components. *Appl. Sci.* **2021**, *11*, 55. [CrossRef]
28. Agrawal, D.; Maheshwari, S. High-performance electronically tunable analog filter using a single EX-CCCII. *Circuits Syst. Signal Process.* **2021**, *40*, 1127–1151. [CrossRef]
29. Roongmuanpha, N.; Faseehuddin, M.; Herencsar, N.; Tangsrirat, W. Tunable mixed-mode voltage differencing buffered amplifier-based universal filter with independently high-*Q* factor controllability. *Appl. Sci.* **2021**, *11*, 9606. [CrossRef]
30. Faseehuddin, M.; Herencsar, N.; Shireen, S.; Tangsrirat, W.; Md Ali, S.H. Voltage differencing buffered amplifier-based novel truly mixed-mode biquadratic universal filter with versatile input/output features. *Appl. Sci.* **2022**, *12*, 1229. [CrossRef]
31. Unuk, T.; Yuce, E. A mixed-mode filter with DVCCs and grounded passive components only. *AEU—Int. J. Electron. Commun.* **2022**, *144*, 154063. [CrossRef]

32. Horng, J.W.; Hou, C.L.; Chang, C.M.; Chou, H.P.; Lin, C.T.; Wen, Y.H. Quadrature oscillators with grounded capacitors and resistors using FDCCIIs. *ETRI J.* **2006**, *28*, 486–493. [CrossRef]
33. Lahiri, A. Novel voltage/current-mode quadrature oscillator using current differencing transconductance amplifier. *Analog Integr. Circuits Signal Process.* **2009**, *61*, 199–203. [CrossRef]
34. Maheshwari, S. Quadrature oscillator using grounded components with current and voltage outputs. *IET Circuits Devices Syst.* **2009**, *3*, 153–160. [CrossRef]
35. Chen, H.P.; Wang, S.F.; Hsieh, M.Y. Tunable current-mode and voltage-mode quadrature oscillator using a DVCCTA. *IEICE Electron. Express* **2014**, *11*, 1–16. [CrossRef]
36. Tangsrirat, W. Dual-mode sinusoidal quadrature oscillator with single CCTA and grounded capacitors. *Inf. MIDEM* **2016**, *46*, 130–135.
37. Srivastaya, M.; Prasad, D. VDCC based dual-mode sinusoidal quadrature oscillator with outputs at appropriate impedance. *Theor. Appl. Electr. Eng.* **2016**, *14*, 168–177. [CrossRef]
38. Tangsrirat, W. Compact quadrature oscillator with voltage and current outputs using only single VDTA and grounded capacitors. *Indian J. Pure Appl. Phys.* **2017**, *55*, 254–260.
39. Kumar, A.; Kushwaha, A.K.; Paul, S.K. Electronically tunable mixed mode quadrature oscillator using DX-MOCCII. *J. Circuits Syst. Comput.* **2021**, *30*, 2150006. [CrossRef]
40. Channumsin, O.; Bhardwaj, K.; Srivastava, M.; Tangsrirat, W.; Petchmaneelumka, W. Single voltage differencing gain amplifier based dual-mode quadrature oscillator using only grounded passive components. *Eng. Lett.* **2022**, *30*, 255–260.
41. Jaikla, W.; Siripruchyanun, M.; Lahiri, A. Resistorless dual-mode quadrature sinusoidal oscillator using a single active building block. *Microelectron. J.* **2011**, *42*, 135–140. [CrossRef]
42. Jin, J.; Wang, C. Current-mode universal filter and quadrature oscillator using CDTAs. *Turk. J. Electr. Eng. Comput. Sci.* **2014**, *22*, 276–286. [CrossRef]
43. Jin, J. Resistorless active SIMO universal filter and four-phase quadrature oscillator. *Arab. J. Sci. Eng.* **2014**, *39*, 3887–3894. [CrossRef]
44. Tuntrakool, S.; Kumngern, M.; Sotner, R.; Herencsar, N.; Suwanjan, P.; Jaikla, W. High Input Impedance Voltage-Mode Universal Filter and Its Modification as Quadrature Oscillator Using VDDDAs. *Indian J. Pure Appl. Phys.* **2017**, *55*, 324–332.
45. Gupta, M.; Arora, T.S. Realization of current mode universal filter and a dual-mode single resistance controlled quadrature oscillator employing VDCC and only grounded passive elements. *Adv. Electr. Electron. Eng.* **2018**, *15*, 833–845. [CrossRef]
46. Kumngern, M.; Khateb, F. Current-mode universal filter and quadrature oscillator using current controlled current follower transconductance amplifiers. *Analog Integr. Circuits Signal Process.* **2019**, *100*, 235–248. [CrossRef]
47. Yucel, F.; Yuce, E. Supplementary CCII based second-order universal filter and quadrature oscillators. *AEU—Int. J. Electron. Commun.* **2020**, *118*, 153138. [CrossRef]
48. Tangsrirat, W.; Pukkalanun, T.; Channumsin, O. Single VDGA-based dual-mode multifunction biquadratic filter and quadrature sinusoidal oscillator. *Inf. MIDEM* **2020**, *50*, 125–136. [CrossRef]
49. Kumngern, M.; Khateb, F.; Kulej, T.; Psychalinos, C. Multiple-input universal filter and quadrature oscillator using multiple-input operational transconductance amplifiers. *IEEE Access* **2021**, *9*, 56253–56263. [CrossRef]
50. Arora, T.S.; Gupta, M.; Gupta, S.N. An explicit output current-mode quadrature sinusoidal oscillator and a universal filter employing only grounded passive components-a minimal realization. *Adv. Electr. Electron. Eng.* **2021**, *19*, 258–271. [CrossRef]
51. Satansup, J.; Tangsrirat, W. CMOS realization of voltage differencing gain amplifier (VDGA) and its application to biquad filter. *Indian J. Eng. Mater. Sci.* **2013**, *20*, 457–464.
52. Taskiran, Z.G.C.; Sedef, H.; Anday, F. Voltage differencing gain amplifier-based nth-order low-pass voltage-mode filter. *J. Circuit Syst. Comp.* **2018**, *27*, 1850089. [CrossRef]
53. Tangsrirat, W.; Pukkalanun, T.; Channumsin, O. Dual-mode multifunction filter realized with single voltage differencing gain amplifier (VDGA). *Eng. Rev.* **2021**, *41*, 1–14. [CrossRef]
54. Channumsin, O.; Tangsrirat, W. Compact electronically tunable quadrature oscillator using single voltage differencing gain amplifier (VDGA) and all grounded passive elements. *Turk. J. Electr. Eng. Comp. Sci.* **2017**, *25*, 2686–2695. [CrossRef]
55. Channumsin, O.; Tangsrirat, W. Voltage differencing gain amplifier-based sinusoidal quadrature oscillator using only two grounded capacitors. *Recent Adv. Electr. Electron. Eng.* **2019**, *12*, 439–444. [CrossRef]
56. Tangsrirat, W.; Channumsin, O.; Pimpol, J. Electronically adjustable capacitance multiplier circuit with a single voltage differencing gain amplifier (VDGA). *Inf. MIDEM* **2019**, *49*, 211–217.
57. Arbel, A.F.; Goldminz, L. Output stage for current-mode feedback amplifiers, theory and applications. *Analog Integr. Circuits Signal Process.* **1992**, *2*, 243–255. [CrossRef]
58. National Semiconductor, LM13600: Dual Operational Transconductance Amplifiers with Linearizing Diodes and Buffers. Available online: https://pdf1.alldatasheet.com/datasheet-pdf/view/8640/NSC/LM13600N.html (accessed on 31 May 2022).
59. Analog Devices, AD844: 60 MHz, 2000 V/μs, Monolithic op amp with Quad Low Noise. Available online: https://www.analog.com/media/en/technical-documentation/data-sheets/AD844.pdf (accessed on 29 June 2022).